
7-1-2017

The Cenomanian–Turonian Boundary in the Northwestern Part of the Adriatic Carbonate Platform (Ćićarija Mtn., Istria, Croatia): Characteristics and Implications

Vlatko Brčić
Croatian Geological Survey

Bosiljka Glumac
Smith College, bglumac@smith.edu

Ladislav Fuček
Croatian Geological Survey

Anita Grizelj
Croatian Geological Survey

Marija Horvat
Croatian Geological Survey

See next page for additional authors

Follow this and additional works at: https://scholarworks.smith.edu/geo_facpubs



Part of the [Geology Commons](#)

Recommended Citation


Brčić, Vlatko; Glumac, Bosiljka; Fuček, Ladislav; Grizelj, Anita; Horvat, Marija; Posilović, Hrvoje; and Mišur, Ivan, "The Cenomanian–Turonian Boundary in the Northwestern Part of the Adriatic Carbonate Platform (Ćićarija Mtn., Istria, Croatia): Characteristics and Implications" (2017). Geosciences: Faculty Publications, Smith College, Northampton, MA.
https://scholarworks.smith.edu/geo_facpubs/152

This Article has been accepted for inclusion in Geosciences: Faculty Publications by an authorized administrator of Smith ScholarWorks. For more information, please contact scholarworks@smith.edu

Authors

Vlatko Brčić, Bosiljka Glumac, Ladislav Fuček, Anita Grizelj, Marija Horvat, Hrvoje Posilović, and Ivan Mišur

The Cenomanian–Turonian boundary in the northwestern part of the Adriatic Carbonate Platform (Ćićarija Mtn., Istria, Croatia): characteristics and implications

Vlatko Brčić¹  · Bosiljka Glumac² · Ladislav Fuček¹ · Anita Grizelj¹ · Marija Horvat¹ · Hrvoje Posilović¹ · Ivan Mišur¹

Received: 16 January 2017 / Accepted: 19 April 2017 / Published online: 29 April 2017
© Springer-Verlag Berlin Heidelberg 2017

Abstract The Cenomanian–Turonian boundary (CTB) in the Ćićarija Mountain region (northern Istria, Croatia) is characterized by calcisphere limestone successions with a firmground and glauconite horizon, bioturbated intervals, tempestites, and slumped structures as well as microbially laminated and organic-rich interbeds deposited in the northwestern part of the intra-Tethyan Adriatic Carbonate Platform (AdCP). Compilation of the results from three studied sections (Vodice–Jelovica, Martinjak and Planik) of litho-, bio-, and microfacies analyses, X-ray diffraction, SEM, EDS, and stable isotope analyses allowed reconstruction of marine paleoenvironmental conditions during this time period. Shallow-marine carbonate deposits of the Milna Formation underlie a drowned-platform succession of the Sveti (Sv.) Duh Formation. The contact between these two formations is sharp and commonly marked by slumped deposits. The Sv. Duh Formation consists of about 100 m of calcisphere wackestone enriched in organic matter. The results of preliminary $\delta^{13}\text{C}$ and $\delta^{18}\text{O}$ stable isotope analyses indicate the influence of the global Oceanic Anoxic Event (OAE2) on the deposition of this carbonate succession. Anoxic and hypoxic conditions in the water column lead to major changes in the shallow-marine carbonate system of the AdCP. Numerous benthic foraminifera declined during that time, but planktonic foraminifera and calcareous dinoflagellates diversified and expanded greatly. The results of this research provide new insights into the character of the

CTB interval in this part of the Tethyan realm. Local and regional synsedimentary tectonics combined with global upper Cretaceous sea-level dynamics allows the correlation of the investigated deeper-marine lithostratigraphic units with OAE2.

Keywords Cenomanian–Turonian · OAE2 · Adriatic Carbonate Platform (AdCP) · Ćićarija Mtn. · Sv. Duh Formation · Glauconite

Introduction

The time period spanning the Cenomanian–Turonian boundary was characterized by profound paleoenvironmental changes at global scale. World-wide consequences of these events have been the focus of new reports and their influence on local to regional depositional systems. For this reason, our current research focuses on upper Cenomanian–lower Turonian carbonate deposits that record temporary drowning of the northwestern part of the intra-Tethyan AdCP.

Globally, the Cenomanian–Turonian boundary interval (about 93.9 My ago; Cohen et al. 2013; Fig. 1a) is marked by an extinction event and turnover in planktonic foraminifera and radiolarians (Caron and Homewood 1983; Huber et al. 1999; Jarvis et al. 1988; Culver and Rawson 2004; Erba 2004; Gebhardt et al. 2010), by a rise in sea level (Hardenbol et al. 1998; Miller et al. 2005; Voigt et al. 2006; Haq 2014; Sames et al. 2016), and by widespread dysoxic to anoxic conditions in the world oceans known as the Oceanic Anoxic Event 2 or OAE2. This event was originally defined by Schlanger and Jenkyns (1976) and described later by many authors (Jenkyns 1980; Schlanger et al. 1987; Arthur et al. 1987, 1988, 1990; Tsikos et al. 2004;

✉ Vlatko Brčić
vlatko.brcic@hgi-cgs.hr

¹ Department of Geology, Croatian Geological Survey, Sachsova 2, 10000 Zagreb, Croatia

² Department of Geosciences, Smith College, Northampton, MA 01063, USA

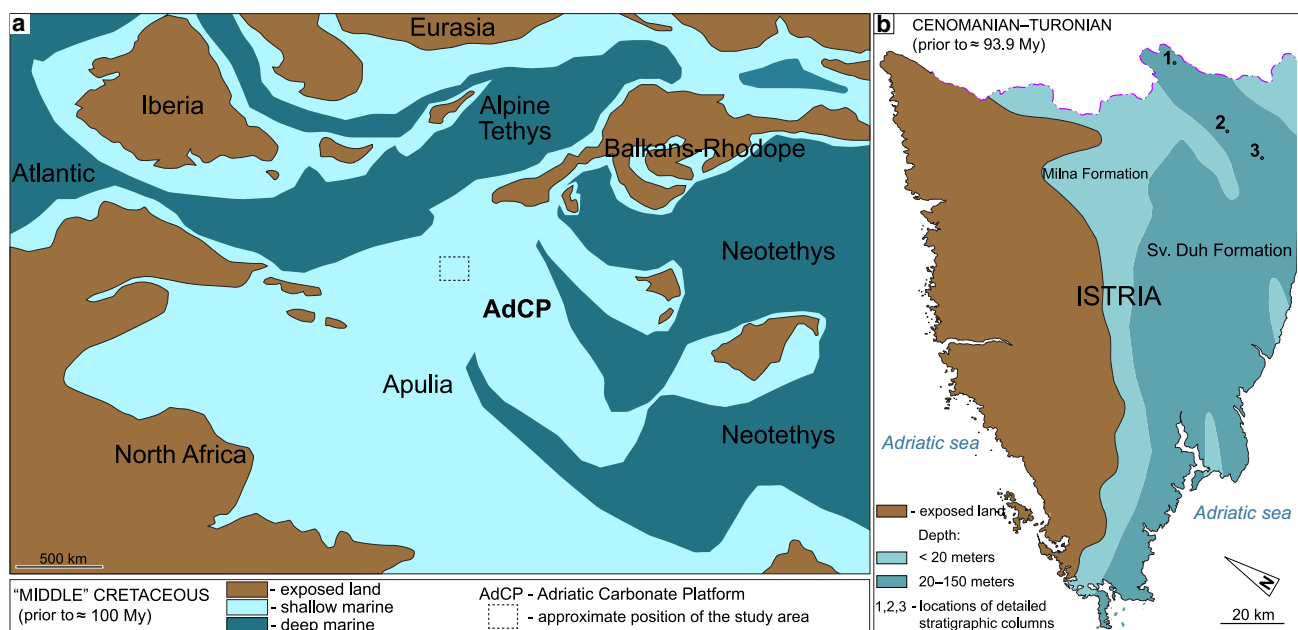


Fig. 1 Paleogeographic reconstructions of the study area. **a** The wider Perimediterranean region prior to approximately 100 Mya with location of the Adriatic Carbonate Platform (AdCP, modified after Blakey 2010; <http://cpgeosystems.com/europaleogeography.html>, and references therein). The *rectangle* outlines the area in the focus of this

study. **b** Depositional environments of Istria during the late Cenomanian to early Turonian (Brčić 2015; the Cenomanian–Turonian time scale according to Cohen et al. 2013). See Fig. 2 for the location of Istria

Keller et al. 2004; Karakitsios et al. 2007, 2010; Pearce et al. 2009; Jenkyns 2010; Jarvis et al. 2011; among others). Successions of OAE2 deposits are mainly represented by uniform deep-marine facies with worldwide distribution (e.g., Eastbourne, England; Rehkogelgraben, Austria; Gubbio, Italy; Tarfaya, Morocco). During the maximum OAE2 about 90% of deep-sea environment on Earth was affected by anoxia (Flögel et al. 2011). The major cause and trigger of a chain reaction that led to anoxic events was interpreted to be submarine volcanism (Larson and Erba 1999; Bralower 2008; Keller 2008; Turgeon and Creaser 2008; Du Vivier et al. 2014; among others). Following the termination of volcanic activity and its input of CO₂, a re-balance of marine environments was gradually achieved. It is estimated that the entire process/event took about 320–960 ky (Sageman et al. 2006) or 500 ky according to Voigt et al. (2008).

Unlike the extensive documentation of the impact of these processes on deep-marine systems, reports on the response of shallow-marine carbonate platform environments are not as numerous (Gušić and Jelaska 1993; Jenkyns 1991; Hilbrecht et al. 1996; Davey and Jenkyns 1999; Immenhauser et al. 2008; Elrick et al. 2009; Gertsch et al. 2010; Nagm 2015). Starting in the early Cenomanian and more profoundly in the middle and late Cenomanian, the stable and uniform shallow-marine AdCP was affected by synsedimentary tectonism and sea-level changes resulting

in episodes of pelagic influence (Tišljär et al. 1998). In some parts of the study area, synsedimentary tectonism overprinted eustatic changes and caused significant paleogeographic differences. As a result, intra-platform basins that formed locally had only occasional pelagic influence of variable intensity (Gušić and Jelaska 1990; Vlahović et al. 1994; Korbar et al. 2012; Brčić 2015). This study, therefore, represents a case study of the relationship between global eustatic trends and local synsedimentary tectonism on shallow-marine carbonate platform facies.

Geological setting

The Adriatic Carbonate Platform (AdCP, Fig. 1a) is one of the largest Mesozoic carbonate platforms of the Perimediterranean region (based on the present-day outcrops from Italy in the northwest to Albania in the southeast, covering an area around 800 × 200 km; Gušić and Jelaska 1993). The entire AdCP carbonate succession was deposited within intra-Tethyan shallow-marine carbonate platform environments and is in places more than 8000 m thick, with a stratigraphic range from the upper part of lower Jurassic (Toarcian) to the Eocene. The end of AdCP deposition was marked by regional emergence between the Cretaceous and the Paleogene (Velić et al. 2002, 2003; Vlahović et al. 2003, 2005; Čosović et al. 2004). The extensive thickness of these

deposits is the result of long-term shallow-marine sedimentation and a series of syndimentary tectonic deformations. Significant structural deformation of the AdCP began in the early Cenomanian, and further intensified in the late Cenomanian (Vlahović et al. 1994; Velić et al. 2003; Brčić 2015; Fig. 1b). Tectonic structure of the Istria Peninsula in the northwestern part of the AdCP reflects these deformations, with the most important phases occurring during the Cretaceous (formation of the western Istrian anticline), and Paleogene (formation of a flysch basin and thrust-nappe structure of the Učka and Čićarija Mountains to the northeast, Fig. 2) (Matičec 1989, 1994; Matičec et al. 1996; Velić et al. 1995). Around the Cenomanian–Turonian boundary, eustatic sea level rise outpaced the rate of carbonate deposition on the AdCP and resulted in the establishment of drowned platform environments (Davey and Jenkyns 1999; Vlahović et al. 2002a, 2005; Korbar et al. 2012).

Study area

The studied outcrops are located in the Mtn. Čićarija region in the northeastern part of Istria, in an area about 45 km long and 10–15 km wide (Fig. 2). The largest part of Mtn. Čićarija is composed of Cretaceous and Paleogene carbonate deposits. The oldest deposits outcropping in the study area are lower Cretaceous (Hauterivian–Albian) limestones and dolomites, overlain by dolomites and post-depositional diagenetic breccia of Albian–Cenomanian age (Vlahović et al. 2002b). The Cenomanian–Turonian deposits are represented by rudist limestones and deeper-marine calcisphere limestones.

Paleogeographically, this area belongs to the northwestern part of the AdCP (Fig. 1a). Present-day western Istria was already emerged during the Cenomanian (Vlahović et al. 1994, 2002a, b; Brčić 2015; Fig. 1b). In other parts of

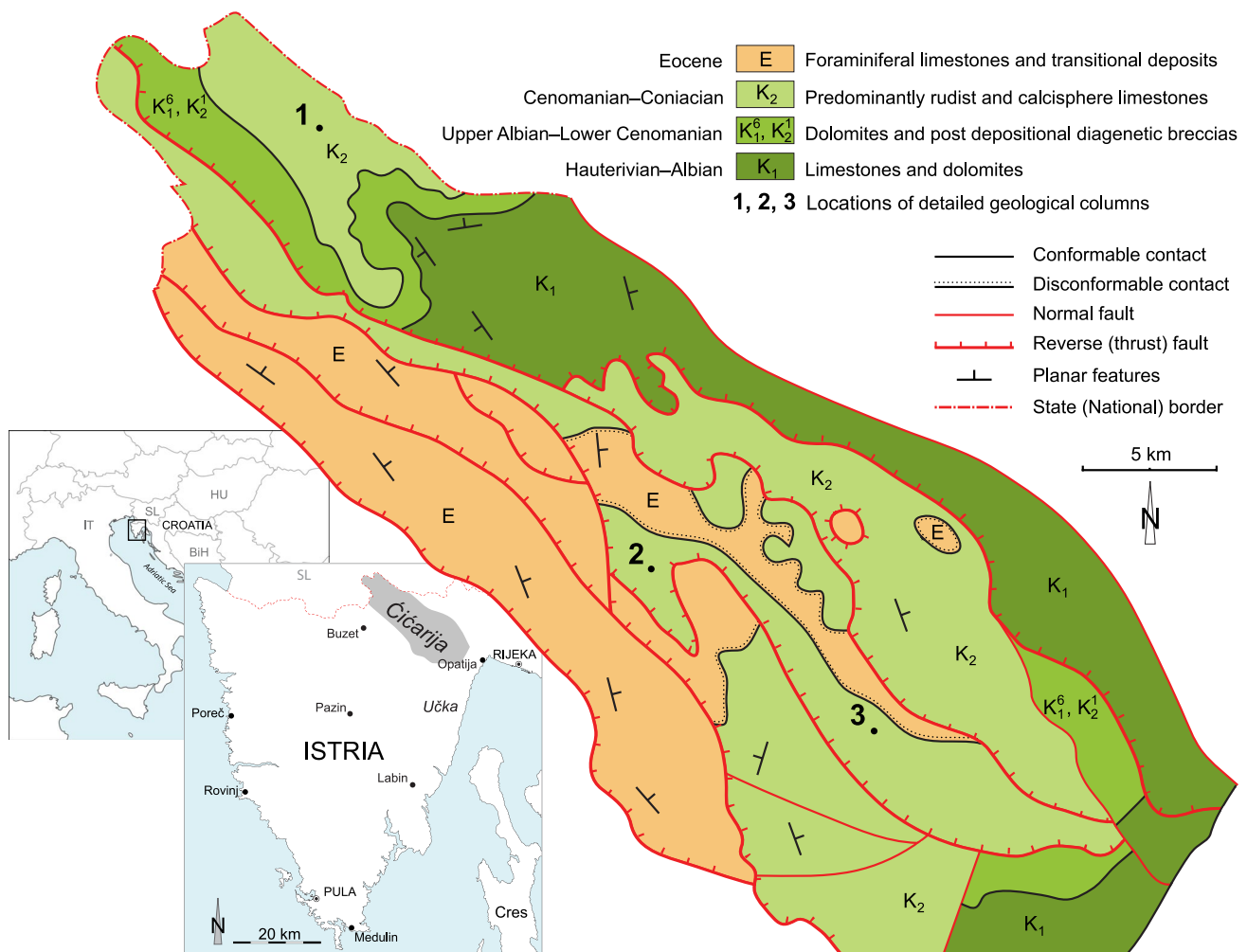


Fig. 2 Geological map of the Čićarija Mtn. area in Istria, Croatia, with positions of detailed geological columns (1 Vodice-Jelovica (45°29′33.929″N, 14°2′13.92419″E), 2 Martinjak (45°23′48.10649″N, 14°8′47.97916″E) and 3 Planik

(45°21′43.23027″N, 14°13′0.55061″E). Modified from the Basic Geological Map of the Republic of Croatia 1:300.000 (Croatian Geological Survey 2009)

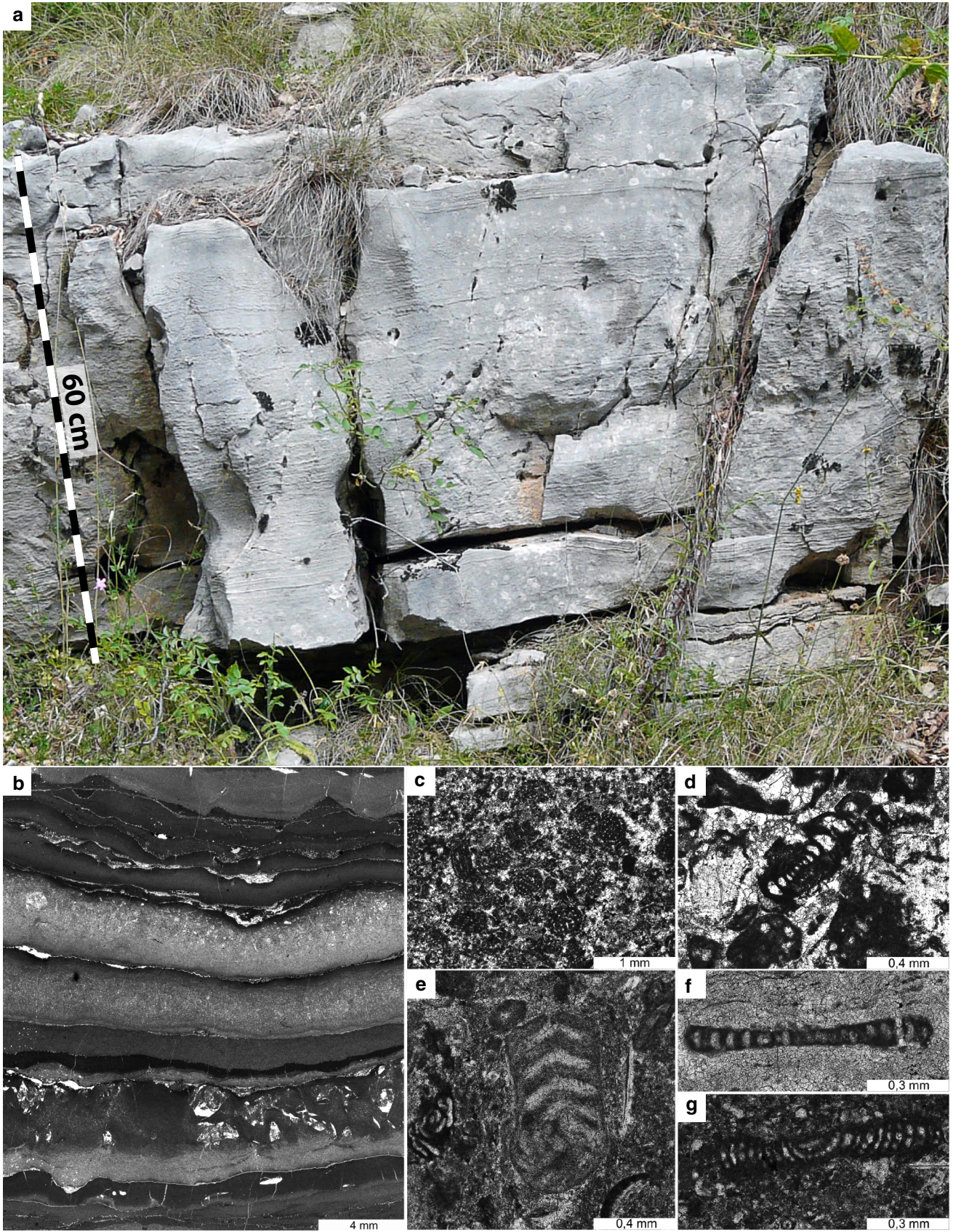


Fig. 3 Outcrop and thin-section photographs of the upper part of the Milna Formation. **a** Microbial laminite (5 m up the Martinjak section). **b** Thin-section photograph of a laminite sample from the outcrop shown in **a**; alternating micrite and microsparite laminae with mouldic porosity (likely evaporite minerals diagenetically replaced with calcite). **c–g** Bioclastic-skeletal packstone interbedded with microbial laminite (top of the outcrop shown in **a**) including fecal pellets (*Favreina* sp.) (**c**) and benthic foraminifera (*Vidalina radoicicae* Cherchi and Schroeder (**d**), *Pseudorhapydionina dubia* (De Castro) (**e**), *Broeckina* (*Pastrikella*) *balcanica* Chierchi et al. (**f**, **g**))

Istria (eastern and northern parts of the present-day peninsula), sedimentation continued into the late Turonian, and in some places until the early Coniacian [with the exception of small areas of the Učka Mtn. and Medulin (Fig. 2) where sedimentation continued until the early Santonian to late Campanian; Brčić 2015]. Between the Coniacian and Eocene, the entire area of the Istrian Peninsula was subaerially exposed.

This study focuses on the deeper-marine Sv. Duh Formation (upper Cenomanian–lower Turonian) bounded by two shallow-marine units, the underlying Milna Formation (lower Cenomanian–upper Cenomanian) and the overlying Gornji Humac Formation (Turonian–Coniacian).

Materials and methods

Stratigraphic columns

Reconnaissance geological field work in the study area identified the best-quality exposures of continuous successions of strata (Fig. 2). The surrounding area was mapped at a scale of 1:25,000. Three detailed stratigraphic sections were measured with a total thickness of about 350 m: the Vodice–Jelovica Sect. (153 m), the Martinjak Sect. (166 m), and the Planik Sect. (32 m). Different rock types were sampled for petrographic and micropaleontological analyses for a total of 116 polished slabs and 163 thin-sections in order to define lithotypes and microfossil assemblages, interpret depositional environments, and document diagenetic modifications.

Stable-isotope geochemistry

Analysis was carried out on a total of 81 samples (Fig. 2). Small amounts of carbonate powder (homogeneous, micritic, and non-weathered material, excluding areas with carbonate cement and skeletal fragments) were collected from polished slabs and thin-section billets using a microscope-mounted microdrill. Stable-isotope analyses were performed using a DeltaXL mass spectrometer (University of Massachusetts, Amherst, USA). After heating for an hour at 400 °C to remove any volatile organic components,

samples were reacted at 70 °C with 100% anhydrous phosphoric acid (H_3PO_4) for 10 min. Standard isobaric and phosphoric acid fractionation corrections were applied to all data. Results are expressed as $\delta^{13}C$ and $\delta^{18}O$ values in ‰ relative to the Vienna PeeDee Belemnite standard (VPDB).

X-ray diffraction and mineralogy of insoluble residue

Mineral composition of insoluble residue from a single sample (glauconite horizon, section Planik) was analyzed by X-ray powder diffraction (XRPD) using a Philips vertical goniometer (experimental conditions: 45 kV, 40 mA, PW 3018/00 PIXcel detector, primary beam divergence $1/4^\circ$, and continuous scan step $0.02^\circ 2\theta/s$). The sample was prepared by dissolving carbonate fraction using acetic acid with an ammonium acetate (1 mol/dm^3) buffer of pH 5, and by sieving the residue to three separate fractions (<0.09 , $0.09\text{--}0.125 \text{ mm}$ and $>0.125 \text{ mm}$).

Scanning electron microscopy (SEM) and energy-dispersive spectroscopy (EDS)

Selected samples were examined by using a JEOL Multi-Purpose scanning microscope (JSM-35). The samples were mounted on a metal stub with an adhesive (graphite tape) and coated with gold (20 keV accelerating potential and 90-mA filament current). A subset of samples was also analyzed for elemental chemical composition by using energy-dispersive spectroscopy (EDS; Oxford Instruments, INCA system).

Results

The Milna Formation

This study included only the upper part of this shallow-marine unit. The Milna Formation consists of well-stratified (rarely massive) rudist and chondrodontid bioclastic floatstone alternating with microbial laminites (with common LLH stromatolites; Fig. 3a, b) and foraminiferal wackestone–packstone (Fig. 3c–g). The middle to late Cenomanian stratigraphic age of these deposits is defined by the presence of benthic foraminifera *Broeckina* (*Pastrikella*) *balcanica* Cherchi et al. *Chrysalidina gradata* D’Orbigny, *Pseudorhapydionina dubia* (De Castro), and *Vidalina radoicicae* Cherchi and Schroeder.

The Sv. Duh Formation

Transition from the Milna Formation into the overlying Sv. Duh Formation can be gradual or sharp. In the case of gradual transition, the laminites (Fig. 3a, b) and/or bioclastic

limestone are replaced with progressively thicker intercalations of calcisphere mudstone-wackestone, whereas in sharp transitions, the well-stratified lithotypes are overlain by massive calcisphere-rich limestone (Fig. 4a).

Thickness of the Sv. Duh Formation in the study area is between 100 and 130 m. Calcisphere limestones of the Sv. Duh Formation are greyish, brownish-greyish to light brown in color, and appear poorly stratified to massive (several meters thick), with stylolites and tectonic fractures. “Mottled intervals” are the result of diagenetic re-distribution and concentration (due to cracks and veins) of organic matter. Other characteristic features of the Sv. Duh deposits include bioturbation, dissolution seams, current microlamination, and nodular appearance of upper bedding planes. Diagenetic processes such as micritization and dolomitization are apparent in thin-sections.

A typical microfacies of the Sv. Duh Formation consists of calcareous dinoflagellate cysts (Fig. 4a) in micritic matrix with variable amounts of fine-grained carbonate bioclasts, planktonic foraminifera (Fig. 4b, c), ostracods, pelagic crinoids, sponge spicules, echinoid spines and rare benthic foraminifera, bivalves, and gastropods. Calcareous detritus mainly derives from shells of rudists, other bivalves and benthic foraminifera. Organic matter is irregularly dispersed as fine opaque particles inside stylolites, bedding planes, cracks, and veins (Fig. 5a–f).

The stratigraphic range of the Sv. Duh Formation is upper Cenomanian–middle Turonian. This is supported by benthic foraminifera from the underlying Milna Formation (Fig. 3d–g) and the presence of planktonic foraminifera *Helvetoglobotruncana helvetica* (Bolli) in the Sv. Duh Formation (Figs. 4b, 5c). In general, deposits of the Sv. Duh are interpreted to represent deeper-marine settings of the temporarily submerged/drowned carbonate platform with a significant open-ocean influence.

The Gornji Humac Formation

Transition between the Sv. Duh and the Gornji Humac Formations is characterized by a shallowing-upward trend. In some cases, the formational boundary is characterized by oncolith and laminite facies. Deposits in the lower part of the Gornji Humac contain shallow-water bioclastic material mainly composed of rudist debris, but benthic foraminifera, echinoid spines, fine carbonate detritus, and peloids are also present. This part of the succession also contains common recrystallized and dolomitized zones. The boundary between the Gornji Humac and Sv. Duh Formations is also characterized by the first appearance of fenestral mudstone with *Decastronema* (*Aeolisacus*) *kotori* (Radoičić) (Fig. 6a) and *Thaumatoporella* sp. (without pelagic influence), followed by peloid-skeletal wackestone, bioclastic-skeletal

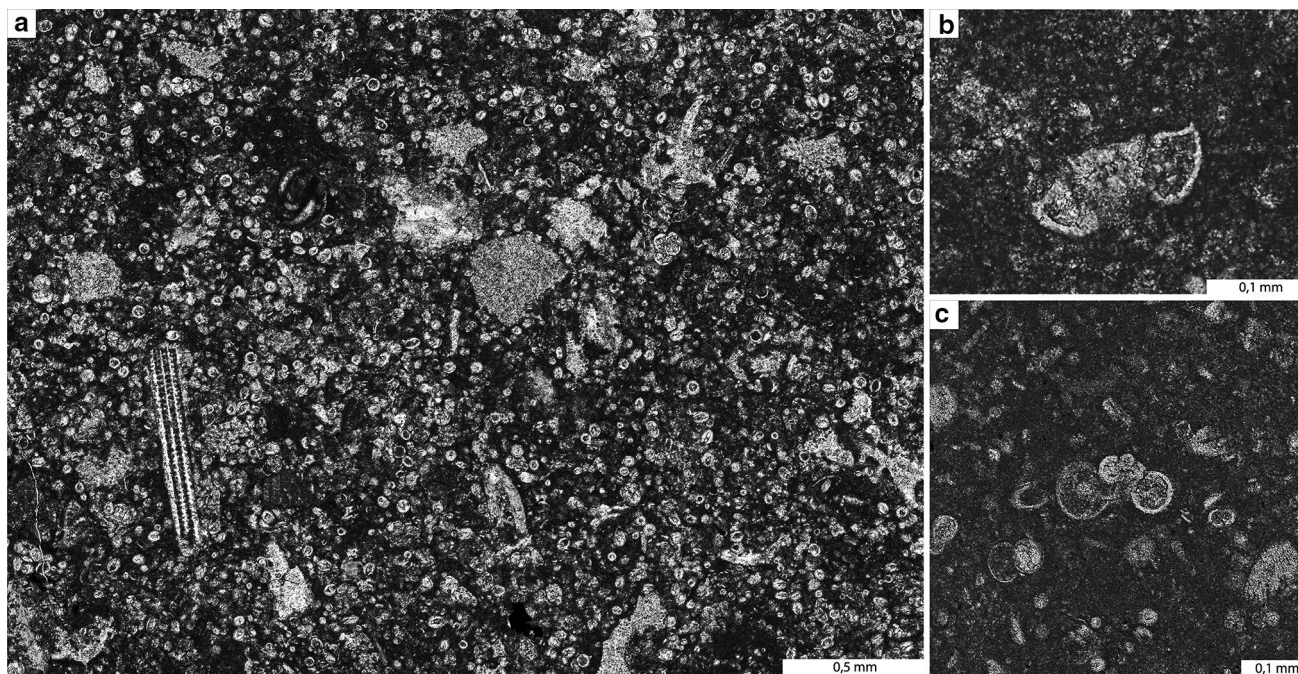


Fig. 4 Thin-section photographs of the Sv. Duh Formation deposits. **a** Microfacies characterized by calcareous dinoflagellate cysts, planktonic foraminifera, and other carbonate bioclasts such as echinoderm remains (10 m up the Vodice–Jelovica section). **b** Relatively

rare planktonic foraminifera *Helvetoglobotruncana helvetica* (Bolli) (23 m up the Planik section). **c** *Whiteinella* cf. *baltica* (Douglas and Rankin) (12 m up the Vodice–Jelovica section)

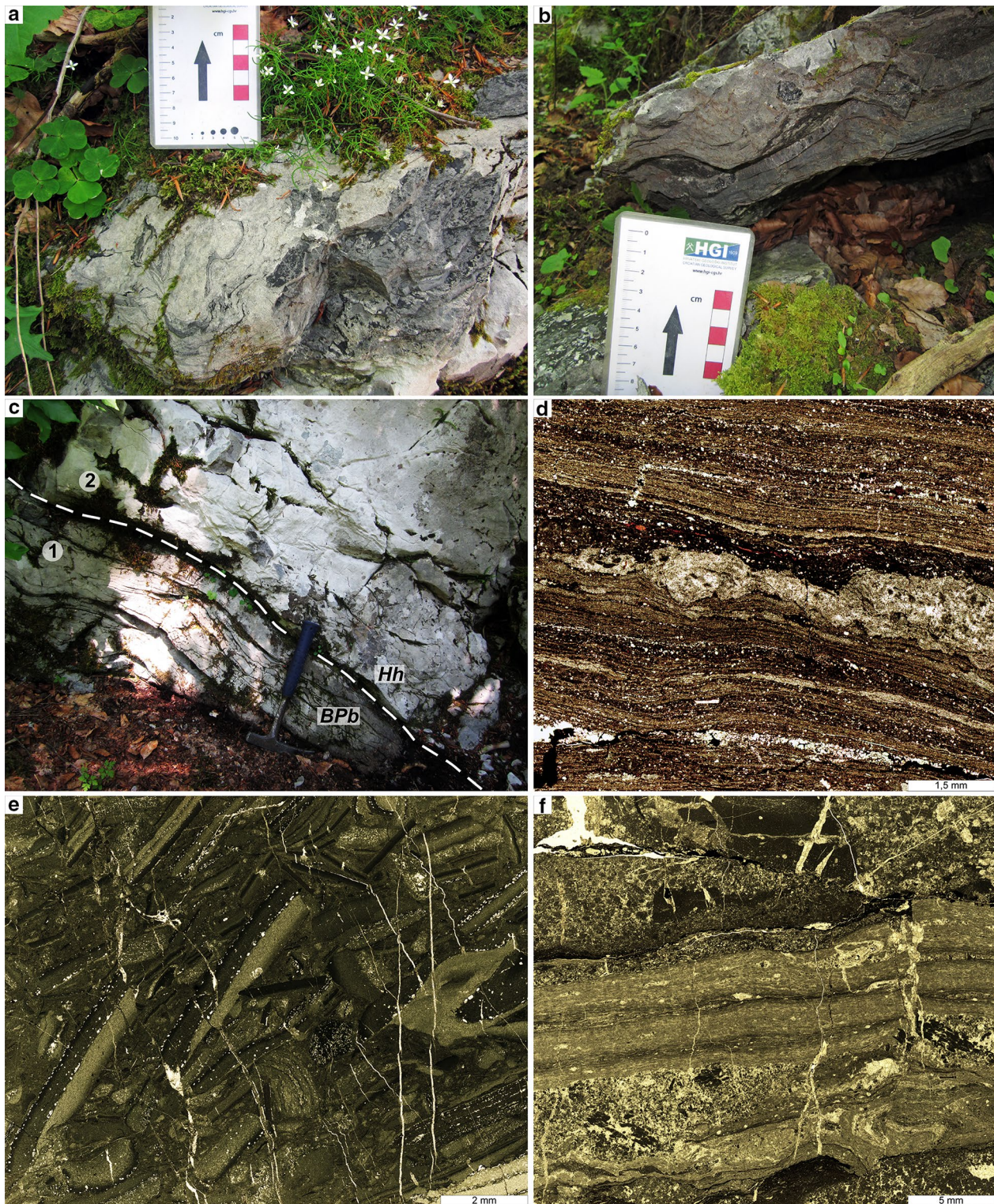


Fig. 5 Outcrop and thin-section photographs of the Cenomanian–Turonian boundary (CTB) in the Sv. Duh Formation (21–23 m up the Planik section). **a–b** Field photograph of microbial laminites enriched in organic matter. **c** Field photograph of CTB (white dashed line) between microbial laminites (1) below and calcisphere mudstone-wackestone (2) above. *BPb* *Broeckina (Patrikella) balcanica*, middle to upper Cenomanian; *Hh* *Helvetoglobotruncana helvetica*, lower

to middle Turonian (*hammer* for scale is 32 cm long). **d** Photomicrograph of microbial laminites enriched in organic matter. **e** Photomicrograph of tempestites with fragmented horizons of euhedral (rhombohedral) forms of dolomite and evaporite dissolution voids now occluded by calcite. **f** Thin-section view of alternating microbial laminites and bioclastic wackestone and packstone with *Favreina* sp., benthic foraminifera and sponge spicules

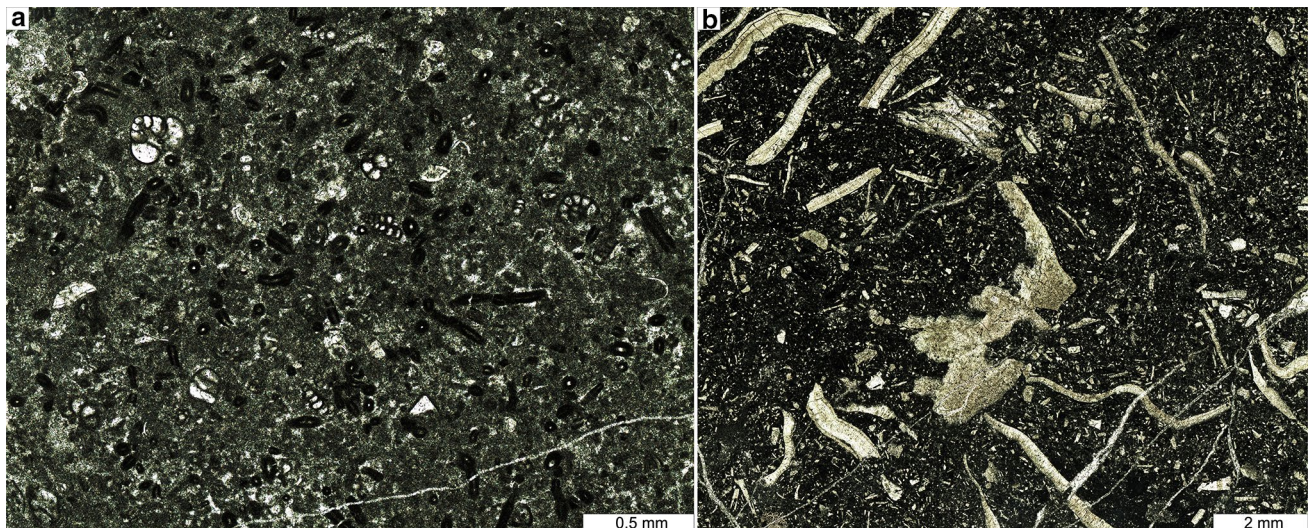


Fig. 6 Thin-section photographs of two typical microfacies of the Gornji Humac Formation. **a** Skeletal-bioclastic packstone with *Decastronema (Aeolisacus) kotori* (60 m up the Vodice–Jelovica sec-

tion). **b** Bioclastic grainstone-floatstone with biodebris composed mainly of rudists shells (118 m up the Vodice–Jelovica section)

wackestone-packstone, intraclastic-skeletal packstone-grainstone, and radiolitid floatstone (Fig. 6b).

The Gornji Humac strata were deposited in moderate to high-energy shallow-water settings and are characterized by lateral changes in sediment size and dominant type of bioclasts. The first index fossils of the Gornji Humac Formation are rudists [*Distefanella* sp. and *Hippurites requieni* (Matheron), Turonian-Coniacian], with subsequent appearance of benthic foraminifera [e.g., *Moncharmontia* sp., *Pseudocyclamina sphaeroidea* (Gendrot), *Scandonea samnitica* De Castro, *S. mediterranea* De Castro, *Dicyclina schlumbergeri* Munier-Chalmas and *Murgella lata* Luperto-Sinni].

Stratigraphic successions and biostratigraphic analyses

Section Vodice–Jelovica

The Vodice–Jelovica section (label *VJe*; thickness 153 m; Fig. 7) was measured in the northwestern part of Čićarija, north of the main road between the villages of Vodice and Jelovica, along the border with Slovenia (2 km northwest of Vodice; Fig. 2).

Interval 0–10 m (*Milna Formation*)

This interval is predominantly made of peloid-skeletal packstone with numerous benthic foraminifera, rudists, oyster bioclasts, fine carbonate detritus, microsparite matrix, and a substantial proportion of organic matter that gives these deposits a dark, bituminous color. The strata are commonly laminated with some bed-parallel stylolites

and microbial laminae (Fig. 3a). In nine selected and analyzed samples the following species of benthic foraminifera were identified: *Chrysalidina gradata* D’Orbigny, *Broekina (Patrikella) balcanica* Cherchi et al. (Figure 3f, g), *Pseudonummolocolina heimi* (Bonet), *Cuneolina pavonia* d’Orbigny, *Nezzazata simplex* Omara, *Vidalina radoicicae* Cherchi and Schroeder (Fig. 3d), *Pseudolituonella reicheli* Marie, *Pseudorhapydionina dubia* (De Castro), and *Nezzazatinella picardi* (Henson).

Interval 10–120 m (*Sv. Duh Formation*)

This interval is predominantly composed of bioclastic-skeletal wackestone in micritic matrix. The most common allochems identified in ten selected samples belong to the following species: *Pithonella ovalis* (Kaufmann), *P. sphaerica* (Bonet), *P. innominate* (Bonet) (Fig. 4a), *Whiteinella* cf. *baltica* Douglas and Rankin (Fig. 4c), *Heterohelix reussi* (Cushman), *Guembelitra* cf. *cenomana* (Keller), *Praeglobotruncana stephani* (Gandolfi), *Muricohedbergella delrioensis* (Carsey), *Guembelitra* sp., *Macroglobigerinelloides* sp., *Praeglobotruncana* sp., *Rotalipora* sp., *Whiteinella* sp., and *Muricohedbergella* sp. The remainder of the samples consists of carbonate biodebris (dominantly of bivalves), echinoid spines, ostracods, sponge spicules, and rare benthic foraminifera. Opaque organic matter is irregularly dispersed within the samples. Wavy and nodular textures are observed along some upper bedding planes of these generally poorly stratified and massive deposits. Transition from the *Sv. Duh* into the Gornji Humac Formation is defined by the first appearance of bioclastic detritus with benthic foraminifera *Dicyclina schlumbergeri* Munier-Chalmas.

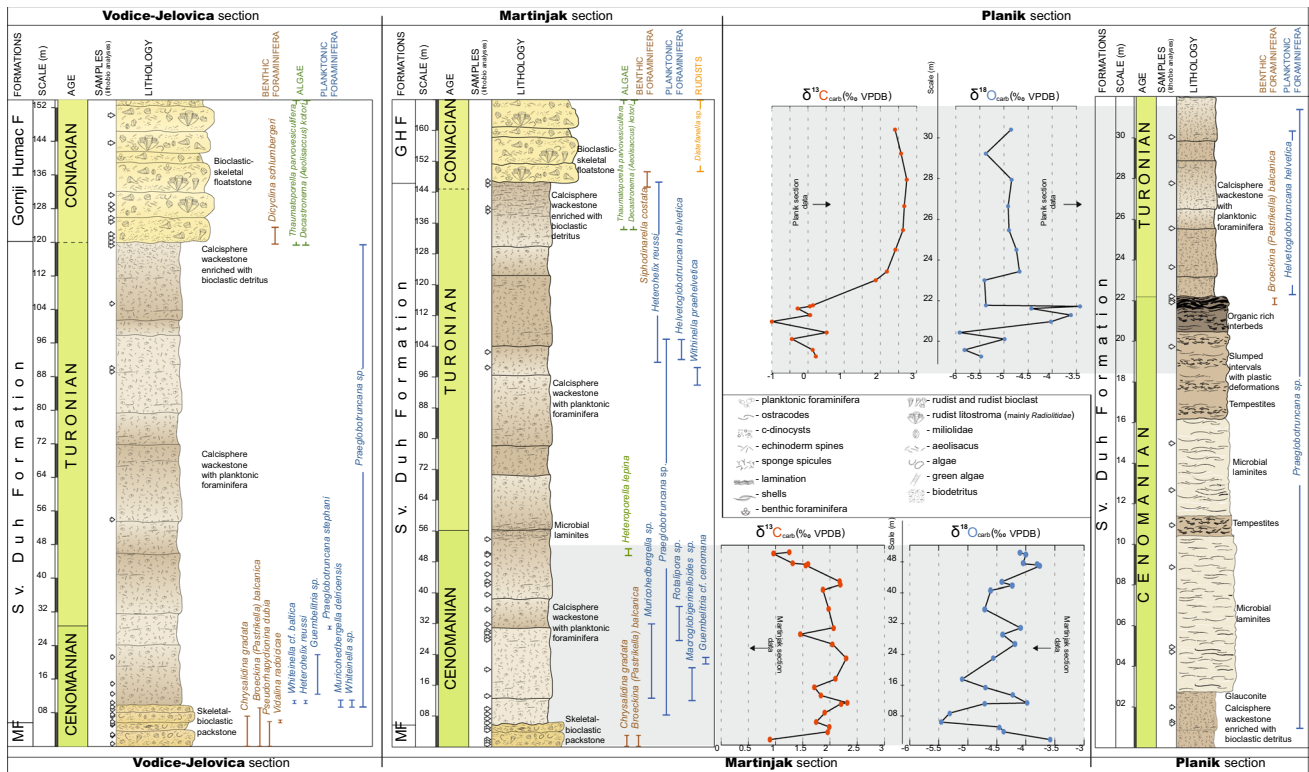


Fig. 7 Detailed measured stratigraphic sections Vodic-Jelovica, Martinjak and Planik from the Čičarija Mtn. in Croatia (see Fig. 2) with $\delta^{13}\text{C}$ and $\delta^{18}\text{O}$ stable isotope data (for the Martinjak and Planik

sections). Notice the different scales among sections. *MF* Milna Formation, *GHF* Gornji Humac Formation

Interval 120–153 m (Gornji Humac Formation)

This interval is predominantly composed of rudist bio-clasts (Fig. 6b), microbial coatings (*Thaumatoporella* sp.), *Decastronema* (*Aeolisacus*) *kotori* Radoičić (Fig. 6a), rare c-dinocysts, planktonic foraminifera, echinoid spines, and sponge spicules. The interval ends with rudist grainstone–floatstone. The Gornji Humac deposits are generally well stratified, with layers ranging from 0.3 to 1.0 m in thickness, and are commonly dolomitized.

Section Martinjak

The Martinjak section (label *Ma*; thickness 150 m; Fig. 7) was measured in the central part of Čičarija Mtn., 1.2 km east of Lanišće (Fig. 2).

Interval 0–5 m (Milna Formation)

This interval is predominantly composed of cyanobacterial laminites with alternating micritic and microsparitic laminae (Fig. 3b) containing euhedral evaporite dissolution moulds now filled with calcite cement. Some of the laminae are dolomitized, and the entire package is slightly slumped.

This interval also contains numerous benthic foraminifera [*Chrysalidina gradata* D’Orbigny, *Broeckina* (*Pastrikella*) *balcanica* Cherchi et al., *Pseudonummoloculina heimi* (Bonet), *Cuneolina pavonia* D’Orbigny, *Nezzazata simplex* Omara, *Vidalina radoicae* Cherchi and Schroeder, *Pseudolituonella reichelli* Marie, *Pseudorhapydionina dubia* (De Castro), *Nezzazatinella picardi* (Henson)], echinoid spines, ostracods, algae [*Decastronema* (*Aeolisacus*) *kotori* (Radoičić)], fecal pellets, microbial coatings, and large shells of gastropods and bivalves.

Interval 5–145 m (Sv. Duh Formation)

This interval contains generally poorly stratified deposits with layer thickness ranging from 0.6 to 1.0 m, with sharp and undulatory bedding planes. Internally, these layers are commonly laminated, and dominated by wackestone composed of fine carbonate detritus with plankton fossils [*Pithonella ovalis* (Kaufmann), *P. sphaerica* (Bonet), *Calcisphaerula innominata* (Bonet), *Heterohelix reussi* (Cushman), *Guembeltria* cf. *cenomana*, *Whiteinella praehelvetica* (Trujillo), *Helvetoglobotruncana helvetica* (Bolli), *Muricohedbergella delrioensis* (Carsey), *Guembeltria* sp., *Macrolobigerinelloides*

Table 1 Results of stable isotope analysis of carbonate samples from the stratigraphic sections Martinjak and Planik including the Cenomanian–Turonian Boundary (CTB) position (*SP* stratigraphic position)

Martinjak				Planik			
Sample	SP (m)	$\delta^{13}\text{C}$ (‰ VPDB)	$\delta^{18}\text{O}$ (‰ VPDB)	Sample	SP (m)	$\delta^{13}\text{C}$ (‰ VPDB)	$\delta^{18}\text{O}$ (‰ VPDB)
M-1	50	1.25	−4.09	P-1	30.1	2.41	−4.85
M-2	49.6	0.96	−4.00	P-2	29	2.57	−5.37
M-3	47.3	1.31	−4.05	P-3	27.8	2.73	−4.84
M-4	47	1.60	−3.82	P-4	26.6	2.66	−4.91
M-5	46.8	1.56	−3.75	P-5	25.5	2.62	−4.89
M-6	42.8	2.18	−4.42	P-6	24.6	2.42	−4.74
M-7	42	2.19	−4.23	P-7	23.6	2.18	−4.68
M-8	40.8	1.87	−4.60	P-8	23.2	1.87	−5.40
M-9	36.2	1.98	−4.71	Lower Turonian			
Lower Turonian				Upper Turonian			
Upper Turonian				P-9	22.05	0.14	−5.37
M-10	31.6	2.06	−4.09	P-10	22	0.06	−3.42
M-II	30	1.45	−4.40	P-II	21.9	−0.29	−4.43
M-12	27.6	2.05	−4.19	P-12	21.6	0.06	−3.61
M-13	24.1	2.30	−4.56	P-13	21.3	−1.00	−4.02
M-14	19	2.10	−5.10	P-14	20.8	0.52	−5.92
M-15	17	1.71	−4.69	P-15	20.5	−0.44	−4.99
M-16	15	1.83	−4.22	P-16	20	0.13	−5.81
M-17	13.2	2.32	−3.98	P-17	19.7	0.22	−5.47
M-18	13	2.21	−4.71				
M-19	10.7	1.90	−5.31				
M-20	8.5	1.75	−5.46				
M-21	7.3	1.99	−4.45				
M-22	6.1	1.96	−4.38				
M-23	4.2	0.90	−3.58				

sp., *Praeglobotruncana* sp., *Rotalipora* sp., *Whiteinella* sp., *Muricohedbergella* sp.], thin-shelled bivalves, echinoid spines and a few large, resedimented shallow-water bioclasts (rudists and gastropods). Dasyclad alga *Heteroporella lepina* Pratulron is also present. The entire interval contains irregularly dispersed organic matter as fine opaque particles inside stylolites, cracks, and veins (Fig. 5d, f).

The upper part of the Sv. Duh Formation at Martinjak is represented by cyanobacterial laminites (with alternating micrite and microsparite), which are sporadically dolomitized and have rare *Pithonella ovalis* (Kaufmann), Heterohelicidae, and globotruncanids. Transition into the Gornji Humac Formation is characterized by an increased proportion of shallow-marine allochems (rudist detritus, large gastropods). Even though the matrix of these deposits still reflects pelagic influence, this interval also has the first appearance of benthic foraminifera *Sifodinarella costata* (Schlagintweit et al. 2014).

Interval 145–150 m (Gornji Humac Formation)

This interval mainly consists of poorly stratified, recrystallized to crystalline, bright yellowish limestones with complete or fragmented shells of rudist. There are also sporadic interlayers of skeletal-bioclastic packstone and bioclastic floatstone with rudist *Distefanella* sp. Also common are algae *Decastronema* (*Aeolisacus*) *kotori* and *Thaumatoporella parvovesiculifera* (Raineri).

Section Planik

The Planik section (label *Pl*; thickness 32 m; Fig. 7) comprises the Sv. Duh Formation and was measured in the central part of Čičarija, along the road Lanišće–Veprinac, 1.8 km northeast of the peak Mali Planik, approximately 900 m above sea level.

The lowermost interval at Planik contains basal deposits of the Sv. Duh Formation (bioclastic-skeletal wackestone–packstone) with shell detritus, echinoid spines, and

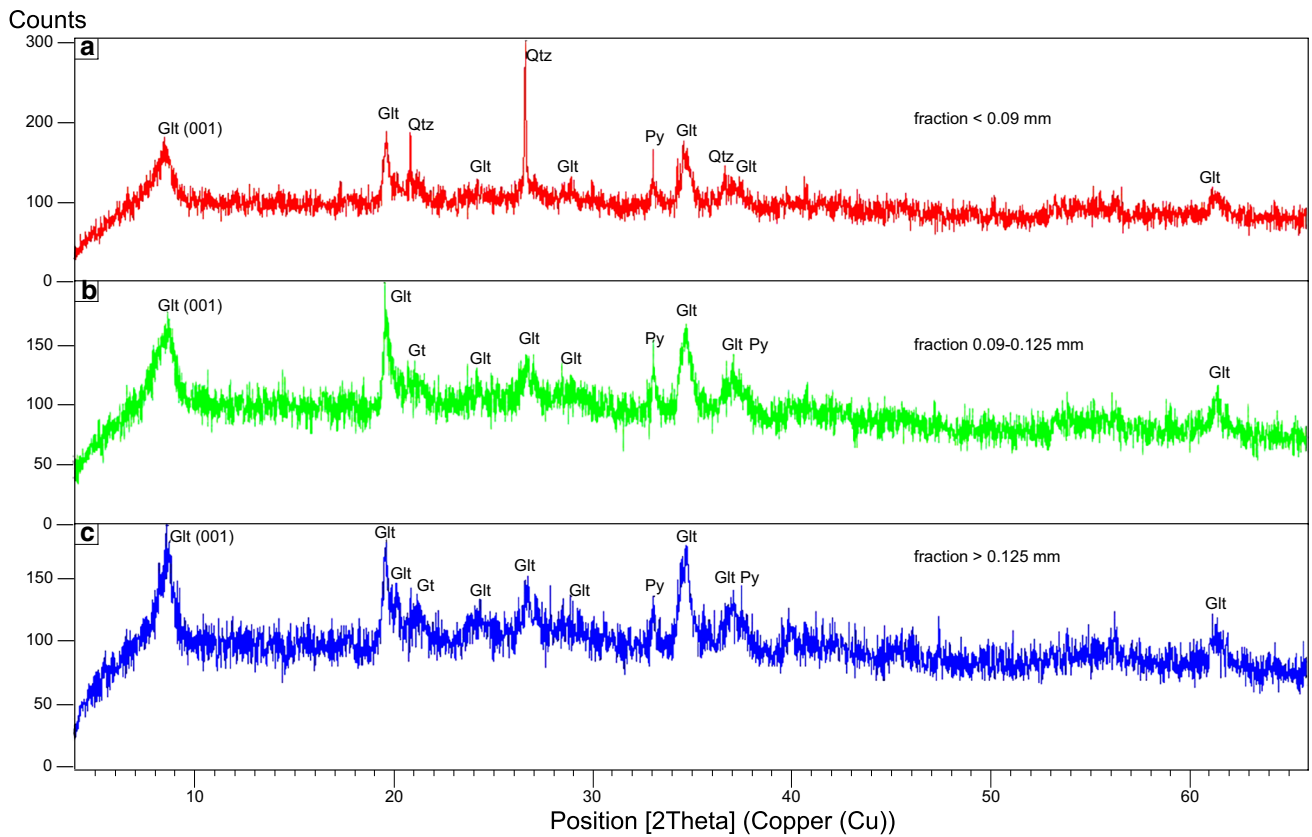


Fig. 8 Comparison of XRPD patterns of insoluble residue of a sample from section Planik (2 m up section). **a** Fraction < 0.09 mm. **b** Fraction 0.09–0.125 mm. **c** Fraction > 0.125 mm. *Glt* glauconite, *Gt* goethite, *Py* pyrite, *Qtz* quartz

other fine biotritus. Pelagic influence is indicated by the presence of *Pithonella ovalis* (Kaufmann), *P. sphaerica* (Bonet), and *Calcisphaerula innominata* Bonet, as well as the planktonic foraminifera *Heterohelix reussi* (Cushman), *Helvetoglobotruncana helvetica* (Bolli) (Fig. 4b), and *Praeglobotruncana* sp.

In general, these deposits are extensively karstified and reveal only poor stratification with massive (over 60 cm thick) layers. The entire interval is bioturbated with several generations of *Thalassinoides*, and contains a visible zone with green to brown glauconite grains, pyrite, and dark to black organic matter.

The section continues upward with slumped cyanobacterial laminites and tempestites (with brittle fractures, but also plastically deformed; Fig. 5a, b, e, f). This zone contains a large proportion of black bituminous organic matter (Fig. 5a, b), and some laminae have shallow-marine skeletal allochems including fecal pellets (*Favreina*; Fig. 3c), and benthic foraminifera [*Broeckina* (*Pastrikella*) *balcanica* Cherchi et al.; Fig. 3f]. Within the laminae there are also common horizons of euhedral dolomite and evaporite (likely anhydrite and gypsum) dissolution moulds filled with calcite cement.

The uppermost part of the succession is composed of bioclastic-skeletal mudstone-wackestone containing fine-grained carbonate detritus, *Pithonella* sp., and planktonic foraminifera [*Helvetoglobotruncana helvetica* (Bolli), *Heterohelicidae*, *Praeglobotruncana* sp., *Muricohedbergella* sp.].

Stable-isotope analysis

Results of carbon and oxygen isotope analysis for carefully selected micritic carbonate samples from the stratigraphic sections Planik and Martinjak are presented in Fig. 7 and Table 1. The sampling was centered around the CTB interval with the intention of comparing the results with the European carbon-isotope reference curve from Eastbourne (Gun Gardens, England; Jarvis et al. 2006; Pearce et al. 2009). In general, relatively narrow compositional ranges were documented for $\delta^{13}\text{C}$ (-1 to $+2.7\text{‰}$) and $\delta^{18}\text{O}$ (-5.9 to -3.6‰) (Fig. 7; Table 1) with no significant covariance between $\delta^{13}\text{C}$ and $\delta^{18}\text{O}$ data, which suggests that the carbon isotope record has not been significantly modified by diagenesis.

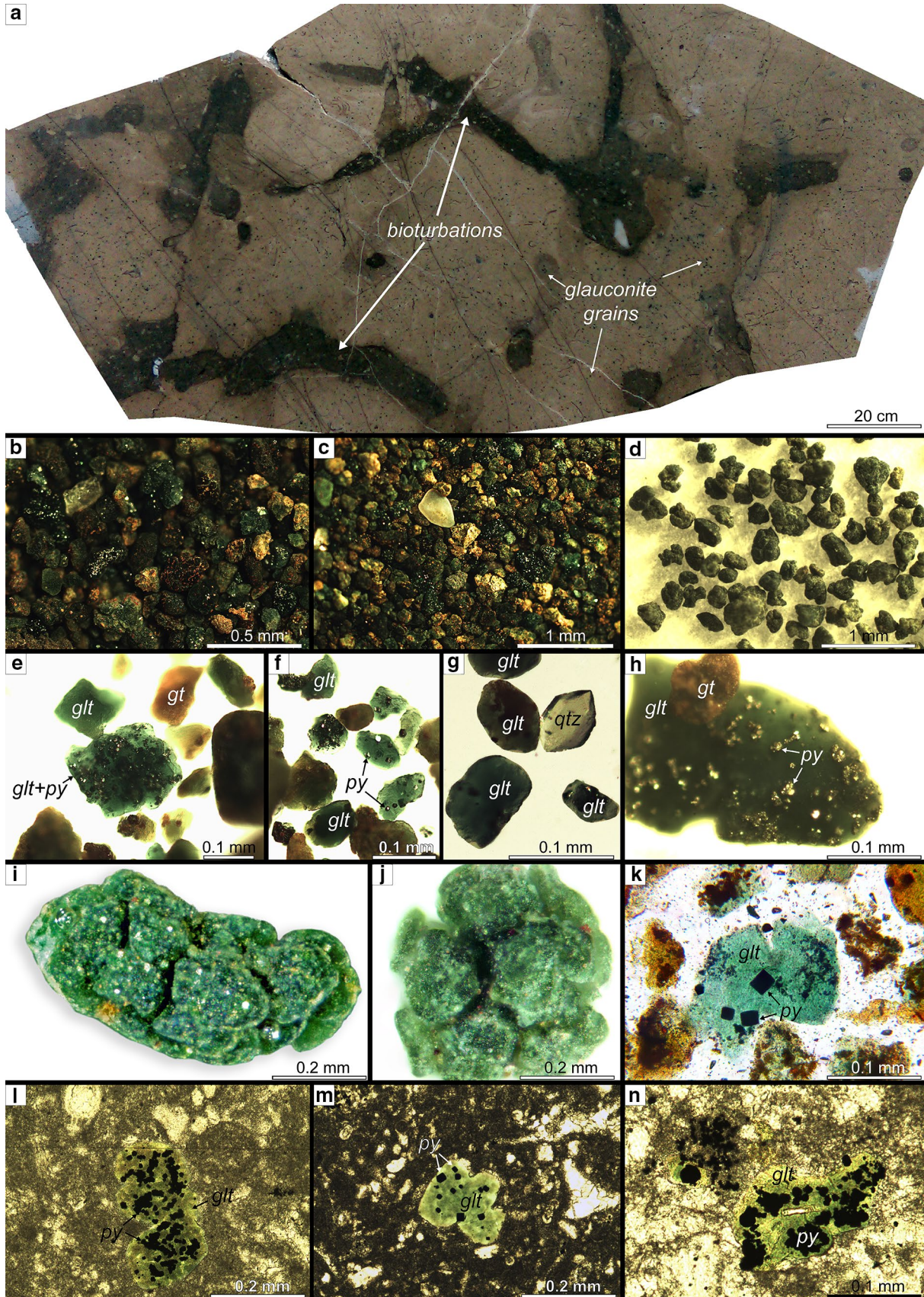


Fig. 9 Samples from the glauconite horizon 2 m up the Planik section. **a** Polished sample of bioturbated (*Thalassinoides*) limestone facies with glauconite grains indicating condensed sedimentation. **b–d** Insoluble residue of the same sample mainly composed of authigenic glauconite grains (three different separates). **e–h** Pyrite inclusions (py) in glauconite grains (glt) with some quartz (qtz) and goethite (gt) present (from different separates). **i–j** Photomicrograph showing morphology of green authigenic globular glauconite “pellets”. **k** Insoluble residue of the same sample in thin-section under polarized light with idiomorphic pyrite (py) inclusions in glauconite (glt) grains. **l–n** Thin-sections of bioturbated bioclastic wackestone-packstone with idiomorphic pyrite (py) inclusions in glauconite (glt) grains

Carbon isotopes ($\delta^{13}C$)

The lowermost 3 m of the Planik succession (Sv. Duh Formation; about 19–22 m stratigraphically) are characterized by variable $\delta^{13}C$ values (between 0.5 and -1%). This is followed by a rapid increase in $\delta^{13}C$ values to 2.5‰ over just 1.5 m of stratigraphic thickness. The values remain uniformly high up to the 28-m level. The uppermost 2 m of section Planik record a slight decline in $\delta^{13}C$ values from 2.7 to 2.4‰ (Fig. 7; Table 1).

Carbonate samples from the Martinjak section show an initial increase from below 1 to around 2‰ in the lowermost part (bottom 3 m) of the analyzed section, followed by generally high and slightly variable values (between about 1.5 and 2.3‰) for most of the section (6–43 m), and a general decline from 2.2 to 1‰ in the uppermost 7 m of the section (Fig. 7; Table 1).

Oxygen isotopes ($\delta^{18}O$)

Carbonate samples from the Planik section show a considerable variation in their $\delta^{18}O$ values from -5.9 (minimum) to -3.6% (maximum) across the lowermost stratigraphic interval (19–24 m). The remaining part of the section records more uniform $\delta^{18}O$ values between -5.4 and -4.7% (Fig. 7; Table 1).

The Martinjak section shows a progressive shift in $\delta^{18}O$ values from -3.5 (maximum) to -5.5% (minimum) within the first 7 m (uppermost Milna Formation) of the succession. The overlying 32 m are characterized by oscillations in values between -5 and -4% (lowermost Sv. Duh Formation). In the uppermost 10 m of the sampled interval, the values generally increase from -4.7 to -3.8% (Fig. 7; Table 1).

X-ray powder diffraction (XRPD) and mineralogical analyses of insoluble residue

The insoluble residue of samples from Planik is almost exclusively composed of glauconite (Fig. 8a–c) and some quartz. Glauconite ranges in color from dark green to light

yellow, and has irregular rounded forms, with numerous inclusions of idiomorphic pyrite (Fig. 9).

In the grain fraction <0.09 mm glauconite is the dominant mineral phase while pyrite and quartz are less abundant (Fig. 8a). The other two fractions (0.09–0.125 and >0.125 mm) also contain glauconite as the dominant mineral phase and pyrite in subordinate amounts (Fig. 8b, c). These two fractions also contain a small amount of goethite.

The observed color of macroscopic glauconite grains, and the intensity and profile of the basal reflection (001) as a function of maturity suggest that glauconite probably belongs to a highly evolved type (Fig. 8a). This type of glauconite formed in sediments that were for long periods of time at the interface between oxidizing and reducing pore-water conditions due to significant breaks in sedimentation (Odin and Matter 1981; Odin and Fullagar 1988; Glenn and Arthur 1990; Amorosi 1995). According to Föllmi (2016), condensed sedimentation may play a role in the formation and accumulation of glauconite. The large amount of pyrite documented here indicates reducing conditions in unconsolidated sediments, whereas the small amount of goethite likely formed through weathering of pyrite (Figs. 8, 9).

Scanning electron microscopy (SEM) and energy-dispersive spectroscopy (EDS) analysis

Quartz grains in the insoluble residue of the sample from the glauconite horizon of Planik are well-developed and preserved euhedral trigonal alpha phase crystals, 20–60 μm in length (Fig. 10a–c). Such crystals are interpreted to form by authigenic precipitation during late diagenesis (Teodorovich 1961; Flügel 2004). Quartz crystal faces in places have preserved rhombohedral moulds or imprints of carbonate crystals, which indicates that silicification post-dated carbonate crystallization. Many quartz crystals are slightly corroded or etched because of changes in geochemical conditions after their crystallization.

Zircons were also found in the same horizon of the Planik section (Fig. 7). Zircon crystal grains are completely unrounded and show a combination of {100} and {110} prisms with one of the {101} pyramids (Pupin 1980; Fig. 10d–f). Crystal unrounded forms and diameters of <0.05 mm suggest short-distance transport.

Pyrite from the same sample is mainly enveloped by glauconite as euhedral crystals (Figs. 9k–n, 10g) and in places oxidized into goethite, but is also present in framboidal forms (Fig. 10h, i). Pyrite framboids (aggregate size ranging 15–30 μm) are commonly interpreted to form in relatively isolated micro-environments with high sulfide concentrations (Wilkin et al. 1996).

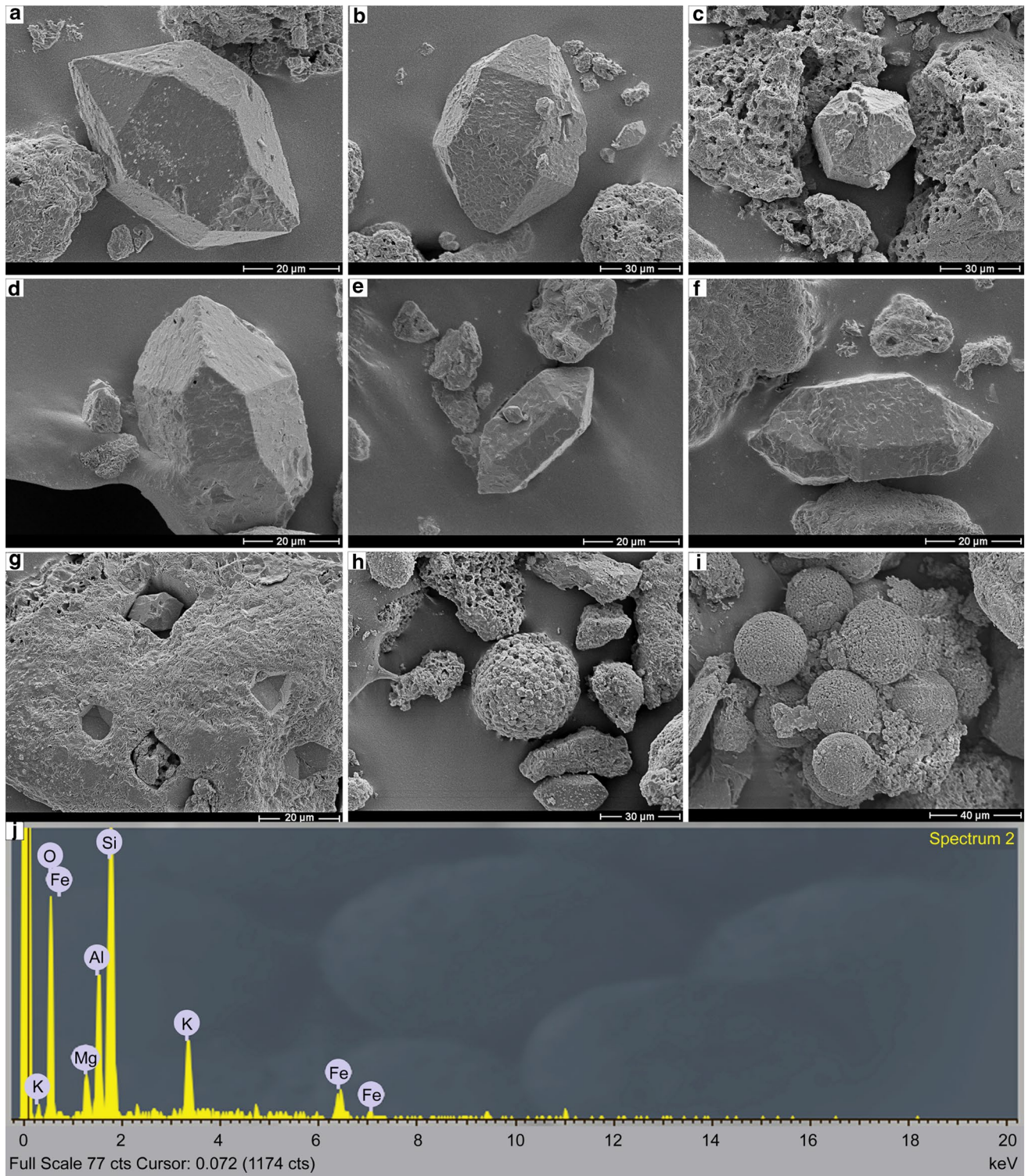


Fig. 10 SEM secondary electron image photomicrographs of the most common minerals in insoluble residue of limestone from the Sv. Duh Formation (2 m up the Planik section). **a–c** Well-developed and slightly corroded authigenic quartz grains. **d–f** Completely unrounded (idiomorphic) crystals of zircon (diameters <0.05 mm, combination of {100} and {110} prisms with either one of the {101} pyramids).

g Layered (mica) structure of glauconite with mouldic porosity (primary euhedral pyrite enveloped by glauconite). **h–i** Framboidal forms of pyrite (aggregate size ranging 15–30 μm). **j** Energy-dispersive spectroscopy (EDS) microanalysis showing elemental composition of layered surface of a single glauconite grain from the Planik section (see **g**)

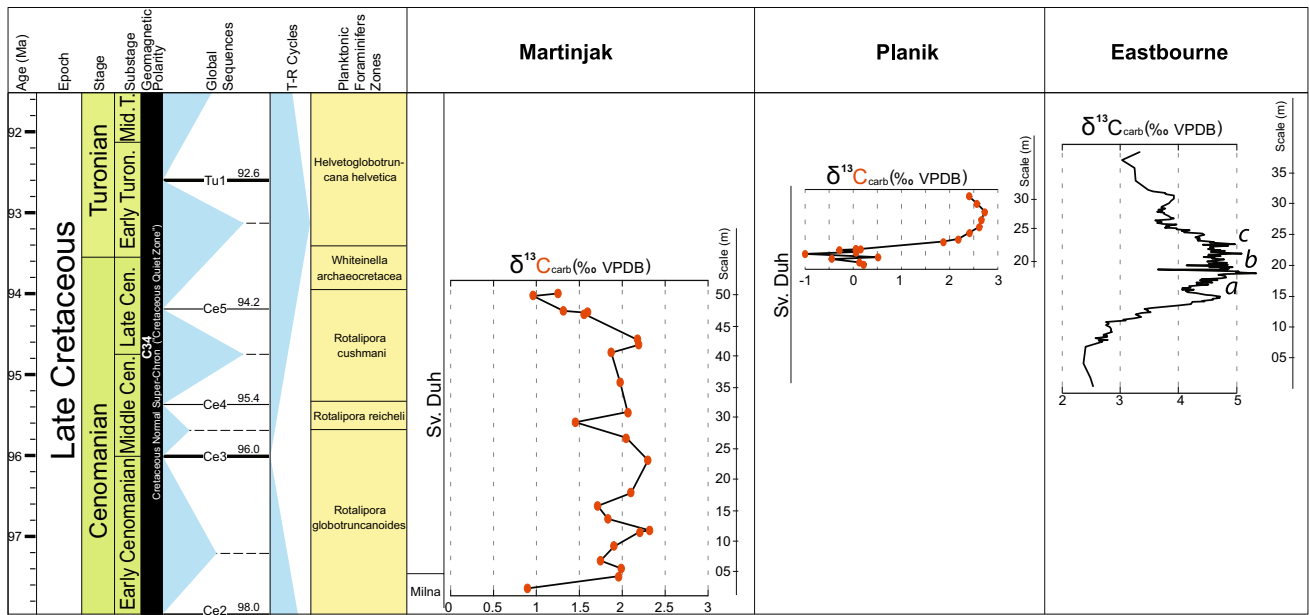


Fig. 11 Chemobiostratigraphic correlation of the Cenomanian–Turonian Martinjak and Planik sections from this study with the reference curve from Eastbourne, Gun Gardens (European reference section, England; Jarvis et al. 2006; Pearce et al. 2009), including the pre-excursion levels, the first build up or peak *a*, the second build-up or peak *b*, the plateau ending with peak *c*, and the recovery of values to the pre-excursion level. The lower part of the Planik curve shows a 3‰ increase in $\delta^{13}\text{C}$ values, which is consistent with a positive shift

towards the excursion plateau levels. The results for the Martinjak section are inconclusive, but the documented increase in $\delta^{13}\text{C}$ values might also be related to the positive excursion at the CTB interval and warrant future detailed chemostratigraphic studies. Geologic time scale from Gradstein et al. (2004) and Ogg et al. (2008), and biochronostratigraphic and sequence chronostratigraphic framework after Hardenbol et al. (1998)

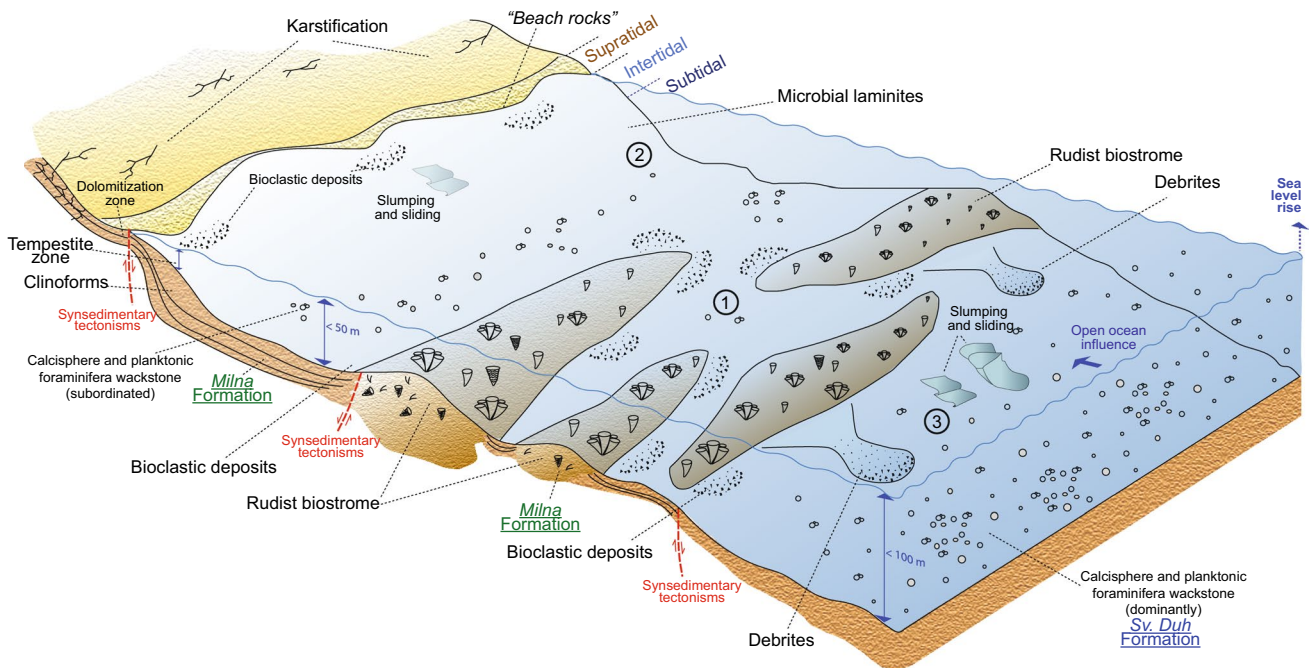


Fig. 12 Block diagram showing the interpretation of the Cenomanian–Turonian depositional environments in the present-day greater Čičarija Mtn. area (former northwestern part of the Adriatic Carbonate Platform; see Fig. 1a, b). A combination of syndepositional tectonisms and global eustatic sea-level rise resulted in the simultane-

ous emersion and deepening of parts of the platform in a relatively close area. Possible relative positions of the formation of deposits from stratigraphic successions Vodice-Jelovica (1), Martinjak (2), and Planik (3)

Discussion

The well-documented Oceanic Anoxic Event 2 (OAE2 or the Bonarelli event; Schlanger and Jenkyns 1976; Tsikos et al. 2004), as well as global eustatic sea level maxima (Haq 2014), left their mark on the shallow-marine carbonate systems of the Adriatic Carbonate Platform (AdCP). The dark, organic carbon-rich limestones of the Sv. Duh Formation (drowned platform facies; Fig. 5a, b) are evidence of oxygen-restricted conditions. The base of this facies is characterized by the appearance of glauconite (Fig. 9a–n), which in conjunction with bioturbation (Fig. 9a), indicates a carbonate factory crisis (Schlager 2003) due to highly reduced carbonate sedimentation rates during that time. Bioturbation enables reactive compounds to become available for sulfate reduction; these compounds would otherwise be destroyed by molecular oxygen at or above the sediment–seawater interface. An important consequence of bacterial sulfate reduction is the formation of syndimentary pyrite (Berner et al. 1985). A significant proportion of pyrite associated with glauconite (Fig. 9e, f, h, k–n) and bioturbation in the Sv. Duh Formation deposits indicate reducing conditions within the sediment prior to lithification.

The color of glauconite grains (Fig. 9i, j) can be used as an indicator of redox conditions, with greenish grains representing less-oxidized conditions in contrast to yellowish grains (Fanning et al. 1989). This is also supported by the more abundant inclusions of pyrite in greenish glauconite grains (Fig. 9e, f, h), which indicate more reducing conditions. The yellowish color of some glauconite grains is due to oxidation of pyrite inclusions and formation of goethite (Fig. 9h, k) as also supported by the results of XRPD analysis (Fig. 8). Such yellowish glauconite grains are more common outside bioturbation infills (Fig. 9a), whereas greenish glauconite grains are predominantly found inside bioturbation infills, additionally supporting the observed relationship between glauconite color and redox levels.

During the Cenomanian and Turonian, there was no significant terrigenous sediment input to the northwestern part of the AdCP. SEM analysis of the insoluble residue from the Planik section has identified the presence of idiomorphic crystals of zircon, <0.05 mm in diameter, suggesting possible eolian transport of pyroclastic material (Fig. 10d–f). The presence of some quartz grains (Fig. 10a–c) and iron as a component of glauconite (Fig. 10j) in these strictly carbonate environments remains an open question. Similarly, the presence of zircon (Fig. 10d–f) opens up the possibility of their age dating in future detailed studies of this stratigraphic interval.

The results of carbon and oxygen isotope analysis (Fig. 7; Table 1) are used to improve stratigraphic

interpretations of these carbonate deposits and for their global correlation. Unlike the relatively nearby OAE2 localities that represent carbonate-free black shales in Italy (Gubio; Coccioni and Luciani 2005), Austria (Rehkegelgraben; Wagneich et al. 2008) and Greece (Ionian zone; Karakitsios et al. 2007, 2010), the examined shallow-marine successions on Čićarija do not contain a considerable amount of non-carbonate components. Even though this preliminary study was limited in the number of samples and in the stratigraphic range of sections within the tectonically highly deformed area of the Čićarija, and some of the scatter in isotope data could be related to contamination from small bioclasts and/or diagenetic modification of micritic matrix (i.e., recrystallization, dissolution and precipitation of calcite cement, and alteration by meteoric fluids; Allan and Matthews 1982; Colombié et al. 2011), the results generally support the presence of the Cenomanian–Turonian boundary event in the examined sections (Fig. 7). This event is represented on the reference Eastbourne Gun Gardens curve (Fig. 11) by the pre-excursion levels, the first build up (or peak *a*, cf. Pearce et al. 2009), the trough, the second build-up (peak *b*), the plateau (ending with peak *c*), and the recovery of $\delta^{18}\text{C}$ values to the pre-excursion levels (Pearce et al. 2009; Fig. 11).

The preliminary results at Martinjak (Fig. 11), hint at the presence of positive carbon isotope excursion at the CTB interval, but remain inconclusive due to the need for more extensive future sampling and analysis of samples from further up section to more completely include the boundary interval. The Planik section, on the other hand, records an increase of about 3‰ in the $\delta^{13}\text{C}$ values consistent with global trends documented for the CTB interval (excursion plateau levels), but just like Martinjak should be more completely sampled and analyzed in the future to include a greater stratigraphic range (Fig. 11).

A late Cenomanian age for the lower part of the Martinjak and Vodice-Jelovica sections is indicated by the presence of benthic foraminifera *Broeckina* (*Pastrikella*) *balcanica* Cherchi et al. (also Planik section), *Vidalina radoicicae* Cherchi and Schroeder and (Fig. 3d, f, g), *Chrysalidina gradata* D'Orbigny, and *Pseudorhapydionina dubia* (De Castro) (upper part of the Milna Formation, CEN-5 zone; Velić and Vlahović 1994, Velić 2007). The Cenomanian genus *Pastrikella* disappeared at the Cenomanian–Turonian boundary (CTB) and was replaced in the late Cretaceous by *Broeckina* (Caus et al. 2013).

Deeper-marine deposits of the Sv. Duh Formation at all three examined sections can be divided into the *Praeglobotruncana* sp. -*Helvetoglobotruncana helvetica* Interval-Zone (late Cenomanian to early Turonian), and *Helvetoglobotruncana helvetica* Partial-range zone

(early-middle Turonian). The first appearance of *Helvetoglobotruncana helvetica* on Planik is directly above the CTB (Fig. 5c).

According to Schlagintweit et al. (2014), benthic foraminifera *Siphodinarella costata* has been recorded so far only from (middle?) Coniacian deposits of the AdCP. It is likely that its stratigraphic range starts in the late Turonian (this paper) or early Coniacian (Schlagintweit et al. 2014).

Integration of carbon-isotope records and detailed biostratigraphy (close vertical ranges of typical late Cenomanian benthic foraminifera and typical early Turonian planktonic foraminifera) allowed a precise determination of the CTB in the study area (Fig. 5c). The documented interaction between synsedimentary tectonics and anoxia on the AdCP has a local to regional character (Gušić and Jelaska 1990; Davey and Jenkyns 1999; Korbar et al. 2012), but it can be correlated with the global OAE2 event (Figs. 11, 12). Synsedimentary tectonics during the CTB (Fig. 12) represents a significant factor in the lateral differentiation of the AdCP facies (Tišljarić et al. 1994, 1998, 2002; Vlahović et al. 1994, 2002a, b, 2005; 2011; Velić et al. 2002, 2003). The main evidence for synsedimentary tectonics is recorded in shallow-marine settings and emerged parts of the western AdCP regardless of the global eustatic sea-level maximum (i.e., emersion horizons developed on shallow-marine Cenomanian deposits of the Milna Formation; Figs. 1b, 12). This research therefore illustrates an example of the global extent of the OAE2 event from open deep-marine to restricted shallow-marine environments.

After the CTB eustatic maximum, intraplatform depressions were filled with bioclastic material from the surrounding areas (Figs. 1b, 12) followed by rapid sea-level fall in the early-middle Turonian interval (Gušić and Jelaska 1993; Miller et al. 2005; Wilmsen et al. 2014). Rudist colonies in the peripheral areas of such depressions were the main source of sediment (best examples are rudist floatstones of the Gornji Humac Formation, Figs. 6b, 12; Korbar et al. 2001). Intensified tectonic activities during the Cenomanian (Fig. 12) marked the beginning of final disintegration of the AdCP, which was once (from Toarcian to Eocene; Vlahović et al. 1994, 2005; Tišljarić et al. 1998) a uniform shallow-marine depositional system.

Conclusions

The three analyzed stratigraphic sections (Vodice-Jelovica, Martinjak and Planik) of Cretaceous carbonate strata of the intra-Tethyan Adriatic Carbonate Platform (AdCP), now exposed in the Čićarija Mountain region (northern Istria, Croatia), show a significant lithological

change between peritidal platform deposits of the Milna Formation and pelagic drowned-platform carbonate deposits of the overlying Sv. Duh Formation. The results of XRD, SEM, EDS, and microfacies analyses of the Planik section deposits documented a glauconite horizon that represents a carbonate factory crisis at the boundary between the Milna and Sv. Duh Formations. Compilation of the results of litho-, bio-, microfacies, and stable isotope analyses indicated the latest Cenomanian to early Turonian age of this event in the Čićarija Mtn. area and illustrated that the globally widespread dysoxic to anoxic conditions associated with the Cenomanian–Turonian boundary, and documented from the deep-marine facies worldwide as the Oceanic Anoxic Event (OAE2), had also impacted the shallow-marine environments of the AdCP. The results of stable isotope analyses of the Martinjak and Planik sections and their comparison with the reference carbon-isotope curve from Eastbourne (Gun Gardens, England) also support the correlation with the OAE2 despite the fact that local synsedimentary tectonism had in places overprinted global eustatic changes and caused significant palaeogeographic differences among depositional settings on the generally shallow-marine northwestern part of the AdCP.

Acknowledgements This work was supported by the Croatian Geological Survey (CGS) and the Ministry of Science, Education and Sports of the Republic of Croatia. We would like to thank two anonymous reviewers and Facies Editor-in-Chief Wolfgang Kiessling for their useful and constructive comments and suggestions that improved the manuscript. Furthermore, Dr. Dubravko Matičec, Dr. Tvrtko Korbar, Dr. Mihovil Briek, MSc. Damir Palenik, and Dr. Tomislav Kurečić from the CGS are thanked for their assistance with field and laboratory analyses, and for offering many valuable suggestions regarding data interpretations and implications. Prof. Stephen Burns (Department of Geosciences, University of Massachusetts, Amherst, USA) is thanked for stable isotope analysis. The first author is also grateful to Prof. Igor Vlahović (Faculty of Mining, Geology and Petroleum Engineering, University of Zagreb, Croatia) for constructive discussions and general advice and support.

References

- Allan JR, Matthews RK (1982) Isotope signatures associated with early meteoric diagenesis. *Sedimentology* 29:797–817
- Amorosi A (1995) Glaucony and sequence stratigraphy: a conceptual framework of distribution in siliciclastic sequences. *J Sediment Res* B65:419–425
- Arthur MA, Schlanger SO, Jenkyns HC (1987) The Cenomanian–Turonian oceanic anoxic event II: palaeoceanographic controls on organic matter production and preservation. In: Brooks J, Fleet A (eds) *Marine petroleum source rocks*, vol 26. Geological Society Special Publication, London, pp 401–420
- Arthur MA, Dean WE, Pratt LM (1988) Geochemical and climatic effects of increased marine organic carbon burial at the Cenomanian/Turonian boundary. *Nature* 335:714–717
- Arthur MA, Brumsack HJ, Jenkyns HC, Schlanger SO (1990) Stratigraphy, geochemistry, and paleoceanography of organic

- carbon-rich Cretaceous sequences. In: Ginsburg RN, Beaudoin B (eds) Cretaceous resources, events, and rhythms. Kluwer Acad. Publ, Netherlands, pp 75–119
- Berner RA, De Leeuw JW, Spiro B, Murchison DG, Eglinton G (1985) Sulphate reduction, organic matter decomposition and pyrite formation. *Philos Trans R Soc Lond Ser A Math Phys Eng Sci* 315(1531):37–38
- Blakey R (2010) <http://jan.ucc.nau.edu/~rcb7/globaltext2.html>. Global Paleogeography. NAU Geology, December 2010
- Bralower TJ (2008) Earth science: volcanic cause of catastrophe. *Nature* 454:285–287
- Brčić V (2015) Relative sea-level changes during the late Cretaceous in the northwestern part of the Adriatic Carbonate Platform. Doctoral Thesis, University of Zagreb, faculty of mining, geology and petroleum engineering, p 229
- Caron M, Homewood P (1983) Evolution of early planktic foraminifers. *Mar Micropaleontol* 7(6):453–462
- Caus E, Parente M, Vicedo V, Frijia G, Martínez R (2013) *Broeckina gassoensis* sp. nov., a larger foraminiferal index fossil for the middle Coniacian shallow-water deposits of the Pyrenean Basin (NE Spain). *Cretac Res* 45:76–90
- Coccioni R, Luciani V (2005) Planktonic foraminifers across the Bonarelli Event (OAE2, latest Cenomanian): the Italian record. *Palaeogeogr Palaeoclimatol Palaeoecol* 224:167–185
- Cohen KM, Finney SC, Gibbard PL, Fan J-X (2013) The ICS international chronostratigraphic chart. *Episodes* 36:199–204
- Colombié C, Lécuyer C, Strasser A (2011) Carbon-and oxygen-isotope records of palaeoenvironmental and carbonate production changes in shallow-marine carbonates (Kimmeridgian, Swiss Jura). Cambridge University Press, Cambridge (**geological magazine**, 148/1:133–153)
- Ćosović V, Drobne K, Moro A (2004) Palaeoenvironmental model for Eocene foraminiferal limestones of the Adriatic carbonate platform (Istrian Peninsula). *Facies* 50:61–75
- Croatian Geological Survey (2009) Geological Map of the Republic of the Croatia scale 1:300.000. HGI-CGS, Department of Geology, Zagreb
- Culver SJ, Rawson PF (2004) Biotic response to global change. The Last 145 million years. Cambridge University Press, The Natural History Museum, London, p 516
- Davey SD, Jenkyns HC (1999) Carbon-isotope stratigraphy of shallow-water limestones and implications for the timing of Late Cretaceous sea-level rise and anoxic events (Cenomanian–Turonian of the peri-Adriatic carbonate platform, Croatia). *Ecolae Geol Helv* 92:163–170
- Du Vivier ADC, Selby D, Sageman BB, Jarvis I, Gröcke DR, Voigt S (2014) Marine $^{187}\text{Os}/^{188}\text{Os}$ isotope stratigraphy reveals the interaction of volcanism and ocean circulation during Oceanic Anoxic Event 2. *Earth Planet Sci Lett* 389:23–33
- Elrick M, Molina-Garza R, Duncan R, Snow L (2009) C-isotope stratigraphy and palaeoenvironmental changes across OAE2 (mid-Cretaceous) from shallow-water platform carbonates of southern Mexico. *Earth Planet Sci Lett* 277:295–306
- Erba E (2004) Calcareous nannofossils and Mesozoic oceanic anoxic events. *Mar Micropaleontol* 52:85–106
- Fanning DS, Rabenhorst MC, May L, Wagner DP (1989) Oxidation state of iron in glauconite from oxidized and reduced zones of soil—geologic columns. *Clay Clay Mine* 37(1):59–64
- Flügel S, Wallmann K, Poulsen CJ, Zhou J, Oschlies A, Voigt S, Kuhnt W (2011) Simulating the biogeochemical effects of volcanic CO_2 degassing on the oxygen–state of the deep ocean during the Cenomanian/Turonian anoxic event (OAE2). *Earth Planet Sci Lett* 305:371–384
- Flügel E (2004) Microfacies of carbonate rocks: analysis, interpretation and application. Springer, Berlin, p 976
- Föllmi KB (2016) Sedimentary condensation. *Earth Sci Rev* 152:143–180
- Gebhardt H, Kuhnt W, Holbourn A (2010) Foraminiferal response to sea level change, organic flux and oxygen deficiency in the Cenomanian of the Tarfaya Basin, southern Morocco. *Mar Micropaleontol* 53(1):133–157
- Gertsch B, Keller G, Adatte T, Berner Z, Kassab AS, Tantawy AAA, El-Sabbagh AM, Stueben D (2010) Cenomanian–Turonian transition in a shallow water sequence of the Sinai, Egypt. *Int J Earth Sci (Geol Rundsch)* 99:165–182
- Glenn CR, Arthur MA (1990) Anatomy and origin of a Cretaceous phosphorite-greensand giant, Egypt. *Sedimentology* 37:123–154
- Gradstein FM, Ogg JG, Smith AG, Agterberg FP, Bleeker W, Cooper RA, Davydov V, Gibbard P, Hinnov LA, House MR, Lourens L, Luterbacher H-P, McArthur J, Melchin MJ, Robb LJ, Sadler PM, Shergold J, Villeneuve M, Wardlaw BR, Ali J, Brinkhuis H, Hilgen FJ, Hooker J, Howarth RJ, Knoll AH, Laskar J, Monechi S, Powell J, Plumb KA, Raffi I, Röhl U, Sanfilippo A, Schmitz B, Shackleton NJ, Shields GA, Strauss H, Van Dam J, Veizer J, Van Kolschoten Th, Wilson D (2004) Geologic time scale 2004. Cambridge University Press, Cambridge, p 589
- Gušić I, Jelaska V (1990) Upper Cretaceous stratigraphy of the Island of Brač. *Djela Jugoslavenske akademije znanosti i umjetnosti Zagreb* 69:160
- Gušić I, Jelaska V (1993) Upper Cenomanian–Lower Turonian sea-level rise and its consequences on the Adriatic–Dinaric carbonate platform. *Geol Rundsch* 82:676–686
- Haq BU (2014) Cretaceous eustasy revisited. *Glob Planet Change* 113:44–58
- Hardenbol J, Thierry J, Farley MB, Jacquín T, Graciansky PC, Vail P (1998) Mesozoic and Cenozoic sequence chronostratigraphic framework of European Basins. In: Graciansky PC et al (ed) Mesozoic and Cenozoic sequence stratigraphy of European basins, vol 60. SEPM Special Publication, p 3–13 (charts 1–8)
- Hilbrecht H, Frieg C, Tröger KA, Voigt S, Voigt T (1996) Shallow water facies during the Cenomanian–Turonian anoxic event: bio-events, isotopes, and sea level in southern Germany. *Cretac Res* 17(2):229–253
- Huber BT, Leckie RM, Norris RD, Bralower TJ, Cobabe E (1999) Foraminiferal assemblage and stable isotopic change across the Cenomanian–Turonian Boundary in the subtropical North Atlantic. *J Foramin Res* 29(4):392–417
- Immenhauser A, Holmden C, Patterson WP (2008) Interpreting the carbon-isotope record of ancient shallow epiceric seas: Lessons from the Recent. In: Pratt B, Holmden C (eds) Dynamics of epiceric seas, vol 48. Geological Association of Canada, St. John's, pp 137–174 (**special Paper**)
- Jarvis I, Carson GA, Cooper MKE, Hart MB, Leary PN, Tocher BA, Horne D, Rosenfeld A (1988) Microfossil assemblages and the Cenomanian–Turonian (late Cretaceous) oceanic anoxic event. *Cretac Res* 9:2–103
- Jarvis I, Gale A, Jenkyns HC, Pearce MA (2006) Secular variation in Late Cretaceous carbon isotopes: a new $\delta^{13}\text{C}$ carbonate reference curve for the Cenomanian–Campanian (99.6–70.6 Ma). *Geol Mag* 143:561–608
- Jarvis I, Lignum JS, Grocke DR, Jenkyns HC, Pearce MA (2011) Black shale deposition, atmospheric CO_2 drawdown, and cooling during the Cenomanian–Turonian Oceanic Anoxic Event. *Paleoceanography* 26:2011–2081
- Jenkyns HC (1980) Cretaceous anoxic events: from continents to oceans. *J Geol Soc Lond* 137:171–188
- Jenkyns HC (1991) Impact on cretaceous sea level rise and anoxic events on the Mesozoic carbonate platform of Yugoslavia. *The Am Asso Pet Geol Bull* 75(6):1007–1017
- Jenkyns HC (2010) Geochemistry of oceanic anoxic events. *Geochem Geophys Geosyst* 11(3):1–30

- Karakitsios V, Tsikos H, Van Bruegel Y, Koletti L, Sinninghe Damsté SJ, Jenkyns HC (2007) First evidence for the Cenomanian–Turonian oceanic anoxic event (OAE2, “Bonarelli” event) from the Ionian Zone, western continental Greece. *Int J Earth Sci (Geol. Rundsch.)* 96:343–352
- Karakitsios V, Kafousia N, Tsikos H (2010) A review of oceanic anoxic events as recorded in the Mesozoic sedimentary record of mainland Greece. *Hell J Geosc* 45:123–132
- Keller G (2008) Cretaceous climate, volcanism, impacts and biotic effects. *Cretac Res* 29:754–771
- Keller G, Berner Z, Adatte T, Stueben D (2004) Cenomanian–Turonian and $\delta^{13}\text{C}$, and $\delta^{18}\text{O}$, sea level and salinity variations at Pueblo, Colorado. *Palaeogeogr Palaeoclimatol Palaeoecol* 211:19–43
- Korbar T, Fuček L, Husinec A, Vlahović I, Oštrić N, Matičec D, Jelaska V (2001) Cenomanian carbonate and rudists along shallow intraplatform basin margin—the Island of Cres (Adriatic Sea, Croatia). *Facies* 45:39–58
- Korbar T, Glumac B, Cvetko-Tešović B, Cadieux SB (2012) Response of a carbonate platform to the Cenomanian–Turonian drowning and OAE 2: a case study from the Adriatic Platform (Dalmatia, Croatia). *J Sediment Res* 82:163–176
- Larson RL, Erba E (1999) Onset of the mid-Cretaceous greenhouse in the Barremian–Aptian: igneous events and the biological, sedimentary, and geochemical responses. *Paleoceanography* 14(6):663–678
- Matičec D (1989) Strukturni sklop područja Rovinj–Poreč (zapadna Istra). M. Sc. Thesis, Faculty of Science, University of Zagreb, pp 50
- Matičec D (1994) Neotectonic deformations in Western Istria, Croatia. *Geol Croat* 47(2):199–204
- Matičec D, Vlahović I, Velić I, Tišljarić J (1996) Eocene limestones overlying lower Cretaceous deposits of Western Istria (Croatia): did some parts of present Istria form land during the Cretaceous? *Geol Croat* 49(1):117–127
- Miller KG, Komazin MA, Browning JV, Wright JD, Mountain GS, Katz ME, Sugarman PJ, Cramer BS, Christie-Blick N, Pekar SF (2005) The Phanerozoic record of global sea-level change. *Science* 310(5752):1293–1298
- Nagm E (2015) Stratigraphic significance of rapid faunal change across the Cenomanian–Turonian boundary in the Eastern Desert, Egypt. *Cret Res* 52:9–24
- Odin GS, Fullagar PO (1988) Geological significance of the glaucony facies. In: Odin GS (ed) *Green marine clays. Developments in sedimentology*, vol 45. Elsevier, Amsterdam, pp 295–332
- Odin GS, Matter A (1981) De glauconiarum origine. *Sedimentology* 28:611–641
- Ogg JG, Ogg G, Gradstein FM (2008) *The concise geologic time scale*. Cambridge University Press, Cambridge, p 150
- Pearce MA, Jarvis I, Tocher BA (2009) The Cenomanian–Turonian event, OAE2 and palaeoenvironmental change in epicontinental seas: new insights from the dinocyst and geochemical records. *Palaeogeogr Palaeoclimatol Palaeoecol* 280:207–234
- Pupin JP (1980) Zircon and granite petrology. *Contrib Mineral Petrol Berl Heidelberg* 73:207–220
- Sageman BB, Meyers SR, Arthur MA (2006) Orbital time scale and new C–isotope record for Cenomanian–Turonian boundary stratotype. *Geology* 34(2):125–128
- Sames B, Wagreich M, Wendler JE, Haq BU, Conrad CP, Melinte-Dobrinescu MC, Hug X, Wendler I, Wolfgring E, Yilmaz İÖ, Zorina SO (2016) Review: short-term sea-level changes in a greenhouse world—A view from the Cretaceous. *Palaeogeogr Palaeoclimatol Palaeoecol* 441:393–411
- Schlager W (2003) Benthic carbonate factories of the Phanerozoic. *Int J Earth Sci* 92:445–464
- Schlagintweit F, Husinec A, Jež J (2014) *Siphodinarella costata* n. gen., n. sp., a new benthic foraminifer from the Coniacian of the Adriatic Carbonate Platform (Slovenia, Croatia). *Facies* 60:133–145
- Schlanger SO, Jenkyns HC (1976) Cretaceous anoxic events: causes and consequences. *Geol Mijnb* 55(3–4):179–184
- Schlanger SO, Arthur MA, Jenkyns HC, Scholle PA (1987) The Cenomanian–Turonian oceanic anoxic event, I. Stratigraphy and distribution of organic-rich beds and the marine $\delta^{13}\text{C}$ excursion. In: Brooks J, Fleet AJ (eds) *Marine petroleum source rocks*, vol 26. Geological Society, London, pp 371–399 (**special publication**)
- Teodorovich GI (1961) Authigenic minerals in sedimentary rocks. Consultants Bureau, New York, p 120
- Tišljarić J, Velić I, Vlahović I (1994) Facies diversity of the Malmian platform carbonates in Western Croatia as a consequence of synsedimentary tectonics. *Géol Méditerr* XXI(3–4):173–176
- Tišljarić J, Vlahović I, Velić I, Matičec D, Robson J (1998) Carbonate facies evolution from the Late Albian to Middle Cenomanian in Southern Istria (Croatia): influence of synsedimentary tectonics and extensive organic carbonate production. *Facies* 38:137–152
- Tišljarić J, Vlahović I, Velić I, Sokač B (2002) Carbonate platform megafacies of the Jurassic and Cretaceous deposits of the Karst Dinarides. *Geol Croat* 55(2):139–170
- Tsikos H, Jenkyns HC, Walsworth-Bell B, Petrizzo MR, Forster A, Kolonic S, Erba E, Premoli Silva I, Bass M, Wagner T, Sinninghe Damsté JS (2004) Carbon-isotope stratigraphy recorded by the Cenomanian–Turonian oceanic anoxic event: correlation and implications based on three key-localities. *J Geol Soc Lond* 161:711–720
- Turgeon SC, Creaser RA (2008) Cretaceous oceanic anoxic event 2 triggered by a massive magmatic episode. *Nature* 454:323–326
- Velić I (2007) Stratigraphy and paleobiogeography of Mesozoic Benthic Foraminifera of the Karst Dinarides (SE Europe). *Geol Croat* 60(1):1–114
- Velić I, Vlahović I (1994) Foraminiferal assemblages in the Cenomanian of the Buzet-Savudrija Area (Northwestern Istria, Croatia). *Geol Croat* 47(1):25–43
- Velić I, Tišljarić J, Matičec D, Vlahović I (1995) Opći prikaz geološke građe Istre. In: Vlahović, I, Velić, I (eds) *First Croatian Geological Congress (Opatija 1995)—Proceedings*, p 5–21
- Velić I, Tišljarić J, Vlahović I, Matičec D, Korbar T, Moro A, Čosović V (2002) Geological evolution of Istria (NW part of the Adriatic Carbonate Platform, Croatia). In: Vlahović, I, Korbar, T (ed.) *6th International Congress on Rudists, Rovinj. Abstracts and Excursion Guidebook*, Zagreb, pp 83–93
- Velić I, Tišljarić J, Vlahović I, Matičec D, Bergant S (2003) Evolution of the Istrian part of the Adriatic Carbonate Platform from the Middle Jurassic to the Santonian and Formation of the Flysch Basin During the Eocene: main events and regional comparison. *Field Trip Guidebook*. In: 22nd IAS Meeting of Sedimentology, Opatija, 17–19 September, Zagreb, p 3–18
- Vlahović I, Tišljarić J, Velić I (1994) Influence of synsedimentary tectonics and eustatic changes on depositions of the Cenomanian platform carbonates in Istria (Western Croatia). *Geol Mediterr* 21(3–4):189–193
- Vlahović I, Korbar T, Moro A, Velić I, Skelton PW, Fuček L, Tišljarić J (2002a) Latest Cenomanian to earliest Turonian platform drowning and Turonian recovery of shallow-water platform deposition in southern Istria. In: *Abstracts and excursion guidebook, sixth international congress on Rudists (Rovinj, Croatia)*, p 152
- Vlahović I, Tišljarić J, Fuček L, Oštrić N, Prtoljan B, Velić I, Matičec D (2002b) The origin and importance of the dolomite-limestone breccia between the Lower and Upper Cretaceous deposits of

- the Adriatic Carbonate Platform: an example from Čićarija Mt. (Istria, Croatia). *Geolo Croat* 55(1):45–55
- Vlahović I, Tišljarić J, Velić I, Matičec D, Skelton PW, Korbar T, Fuček L (2003) Main events recorded in the sedimentary succession of the Adriatic carbonate platform from the Oxfordian to the upper Santonian in Istria (Croatia). Field Trip Guidebook. In: 22nd IAS meeting of sedimentology, Opatija, 17–19 September 2003, p 19–56
- Vlahović I, Tišljarić J, Velić I, Matičec D (2005) Evolution of the Adriatic Carbonate Platform: paleogeography, main events and depositional dynamics. *Paleogeogr Paleoclimatol Paleoecol* 220:333–360
- Vlahović I, Mikša G, Mrinjek E, Hasiotis ST, Velić I, Tišljarić J, Matičec D (2011) Response of tracemakers to temporary platform drowning: lower Cenomanian of Southern Istria (Western Croatia). *Palaios* 26:567–577
- Voigt S, Gale AS, Voigt T (2006) Sea-level change, carbon cycling and palaeoclimate during the Late Cenomanian of northwest Europe; an integrated palaeoenvironmental analysis. *Cretac Res* 27:836–858
- Voigt S, Erbacher J, Mutterlose J, Weiss W, Westerhold T, Wiese F, Wilmsen M, Wonik T (2008) The Cenomanian–Turonian of the Wunstorf section (North Germany): global stratigraphic reference section and new orbital time scale for Oceanic anoxic event 2. *Newsl Stratigr* 43(1):65–89
- Wagreich M, Bojar AV, Sachsenhofer RF, Neuhuber S, Egger H (2008) Calcareous nannoplankton, planktonic foraminifera, and carbonate carbon isotope stratigraphy of the Cenomanian–Turonian boundary section in the Ultrahelvetetic Zone (Eastern Alps, Upper Austria). *Cretac Res* 29:965–975
- Wilkin RT, Barnes HL, Brantley SL (1996) The size distribution of framboidal pyrite in modern sediments: an indicator of redox conditions. *Geochim Cosmochim Acta* 60:3897–3912
- Wilmsen M, Niebuhr B, Janetschke N (2014) Sea-level changes across the Lower-Middle Turonian boundary: evidence from borehole BKS 7/91 (Danubian Cretaceous Group, Bavaria, Germany). *Zeitschrift der Deutschen Gesellschaft für Geowissenschaften* 165:641–654